THE UNIVERSITY OF CALGARY

Numerical Solution of Chemical Absorption of H_2S by an Amine - Containing Spray in Plug Flow, With Cumulative Effects

by

David Strutt

A THESIS

SUBMITTED TO THE FACULTY OF GRADUATE STUDIES

IN PARTIAL FULFILLMENT OF THE REQUIREMENTS FOR THE

DEGREE OF MASTER OF SCIENCE IN ENGINEERING

DEPARTMENT OF CHEMICAL ENGINEERING

CALGARY, ALBERTA

APRIL, 1994

ISBN 0-315-93984-2

Name David Bryan Strutt

Dissertation Abstracts International is arranged by broad, general subject categories. Please select the one subject which most nearly describes the content of your dissertation. Enter the corresponding four-digit code in the spaces provided.

Chemical Engineering
SUBJECT TERM

0542
SUBJECT CODE

U·M·I

Subject Categories

THE HUMANITIES AND SOCIAL SCIENCES

COMMUNICATIONS AND THE ARTS
Architecture 0729
Art History 0377
Cinema 0900
Dance 0378
Fine Arts 0357
Information Science 0723
Journalism 0391
Library Science 0399
Mass Communications 0708
Music 0413
Speech Communication 0459
Theater 0465

EDUCATION
General 0515
Administration 0514
Adult and Continuing 0516
Agricultural 0517
Art 0273
Bilingual and Multicultural 0282
Business 0688
Community College 0275
Curriculum and Instruction 0727
Early Childhood 0518
Elementary 0524
Finance 0277
Guidance and Counseling 0519
Health 0680
Higher 0745
History of 0520
Home Economics 0278
Industrial 0521
Language and Literature 0279
Mathematics 0280
Music 0522
Philosophy of 0998
Physical 0523
Psychology 0525
Reading 0535
Religious 0527
Sciences 0714
Secondary 0533
Social Sciences 0534
Sociology of 0340
Special 0529
Teacher Training 0530
Technology 0710
Tests and Measurements 0288
Vocational 0747

LANGUAGE, LITERATURE AND LINGUISTICS
Language
- General 0679
- Ancient 0289
- Linguistics 0290
- Modern 0291

Literature
- General 0401
- Classical 0294
- Comparative 0295
- Medieval 0297
- Modern 0298
- African 0316
- American 0591
- Asian 0305
- Canadian (English) 0352
- Canadian (French) 0355
- English 0593
- Germanic 0311
- Latin American 0312
- Middle Eastern 0315
- Romance 0313
- Slavic and East European 0314

PHILOSOPHY, RELIGION AND THEOLOGY
Philosophy 0422
Religion
- General 0318
- Biblical Studies 0321
- Clergy 0319
- History of 0320
- Philosophy of 0322

Theology 0469

SOCIAL SCIENCES
American Studies 0323
Anthropology
- Archaeology 0324
- Cultural 0326
- Physical 0327

Business Administration
- General 0310
- Accounting 0272
- Banking 0770
- Management 0454
- Marketing 0338

Canadian Studies 0385
Economics
- General 0501
- Agricultural 0503
- Commerce-Business 0505
- Finance 0508
- History 0509
- Labor 0510
- Theory 0511

Folklore 0358
Geography 0366
Gerontology 0351
History
- General 0578
- Ancient 0579
- Medieval 0581
- Modern 0582
- Black 0328
- African 0331
- Asia, Australia and Oceania 0332
- Canadian 0334
- European 0335
- Latin American 0336
- Middle Eastern 0333
- United States 0337

History of Science 0585
Law 0398
Political Science
- General 0615
- International Law and Relations 0616
- Public Administration 0617

Recreation 0814
Social Work 0452
Sociology
- General 0626
- Criminology and Penology 0627
- Demography 0938
- Ethnic and Racial Studies 0631
- Individual and Family Studies 0628
- Industrial and Labor Relations 0629
- Public and Social Welfare 0630
- Social Structure and Development 0700
- Theory and Methods 0344

Transportation 0709
Urban and Regional Planning 0999
Women's Studies 0453

THE SCIENCES AND ENGINEERING

BIOLOGICAL SCIENCES
Agriculture
- General 0473
- Agronomy 0285
- Animal Culture and Nutrition 0475
- Animal Pathology 0476
- Food Science and Technology 0359
- Forestry and Wildlife 0478
- Plant Culture 0479
- Plant Pathology 0480
- Plant Physiology 0817
- Range Management 0777
- Wood Technology 0746

Biology
- General 0306
- Anatomy 0287
- Biostatistics 0308
- Botany 0309
- Cell 0379
- Ecology 0329
- Entomology 0353
- Genetics 0369
- Limnology 0793
- Microbiology 0410
- Molecular 0307
- Neuroscience 0317
- Oceanography 0416
- Physiology 0433
- Radiation 0821
- Veterinary Science 0778
- Zoology 0472

Biophysics
- General 0786
- Medical 0760

EARTH SCIENCES
Biogeochemistry 0425
Geochemistry 0996
Geodesy 0370
Geology 0372
Geophysics 0373
Hydrology 0388
Mineralogy 0411
Paleobotany 0345
Paleoecology 0426
Paleontology 0418
Paleozoology 0985
Palynology 0427
Physical Geography 0368
Physical Oceanography 0415

HEALTH AND ENVIRONMENTAL SCIENCES
Environmental Sciences 0768
Health Sciences
- General 0566
- Audiology 0300
- Chemotherapy 0992
- Dentistry 0567
- Education 0350
- Hospital Management 0769
- Human Development 0758
- Immunology 0982
- Medicine and Surgery 0564
- Mental Health 0347
- Nursing 0569
- Nutrition 0570
- Obstetrics and Gynecology 0380
- Occupational Health and Therapy 0354
- Ophthalmology 0381
- Pathology 0571
- Pharmacology 0419
- Pharmacy 0572
- Physical Therapy 0382
- Public Health 0573
- Radiology 0574
- Recreation 0575
- Speech Pathology 0460
- Toxicology 0383

Home Economics 0386

PHYSICAL SCIENCES
Pure Sciences
Chemistry
- General 0485
- Agricultural 0749
- Analytical 0486
- Biochemistry 0487
- Inorganic 0488
- Nuclear 0738
- Organic 0490
- Pharmaceutical 0491
- Physical 0494
- Polymer 0495
- Radiation 0754

Mathematics 0405
Physics
- General 0605
- Acoustics 0986
- Astronomy and Astrophysics 0606
- Atmospheric Science 0608
- Atomic 0748
- Electronics and Electricity 0607
- Elementary Particles and High Energy 0798
- Fluid and Plasma 0759
- Molecular 0609
- Nuclear 0610
- Optics 0752
- Radiation 0756
- Solid State 0611

Statistics 0463

Applied Sciences
Applied Mechanics 0346
Computer Science 0984
Engineering
- General 0537
- Aerospace 0538
- Agricultural 0539
- Automotive 0540
- Biomedical 0541
- Chemical 0542
- Civil 0543
- Electronics and Electrical 0544
- Heat and Thermodynamics 0348
- Hydraulic 0545
- Industrial 0546
- Marine 0547
- Materials Science 0794
- Mechanical 0548
- Metallurgy 0743
- Mining 0551
- Nuclear 0552
- Packaging 0549
- Petroleum 0765
- Sanitary and Municipal 0554
- System Science 0790

Geotechnology 0428
Operations Research 0796
Plastics Technology 0795
Textile Technology 0994

PSYCHOLOGY
General 0621
Behavioral 0384
Clinical 0622
Developmental 0620
Experimental 0623
Industrial 0624
Personality 0625
Physiological 0989
Psychobiology 0349
Psychometrics 0632
Social 0451

Nom _____

Dissertation Abstracts International est organisé en catégories de sujets. Veuillez s.v.p. choisir le sujet qui décrit le mieux votre thèse et inscrivez le code numérique approprié dans l'espace réservé ci-dessous.

SUJET	CODE DE SUJET
	☐☐☐ U·M·I

Catégories par sujets

HUMANITÉS ET SCIENCES SOCIALES

COMMUNICATIONS ET LES ARTS

Architecture 0729
Beaux-arts 0357
Bibliothéconomie 0399
Cinéma 0900
Communication verbale 0459
Communications 0708
Danse 0378
Histoire de l'art 0377
Journalisme 0391
Musique 0413
Sciences de l'information 0723
Théâtre 0465

ÉDUCATION

Généralités 515
Administration 0514
Art 0273
Collèges communautaires 0275
Commerce 0688
Économie domestique 0278
Éducation permanente 0516
Éducation préscolaire 0518
Éducation sanitaire 0680
Enseignement agricole 0517
Enseignement bilingue et multiculturel 0282
Enseignement industriel 0521
Enseignement primaire. 0524
Enseignement professionnel 0747
Enseignement religieux 0527
Enseignement secondaire 0533
Enseignement spécial 0529
Enseignement supérieur 0745
Évaluation 0288
Finances 0277
Formation des enseignants 0530
Histoire de l'éducation 0520
Langues et littérature 0279
Lecture 0535
Mathématiques 0280
Musique 0522
Orientation et consultation 0519
Philosophie de l'éducation 0998
Physique 0523
Programmes d'études et enseignement 0727
Psychologie 0525
Sciences 0714
Sciences sociales 0534
Sociologie de l'éducation 0340
Technologie 0710

LANGUE, LITTÉRATURE ET LINGUISTIQUE

Langues
- Généralités 0679
- Anciennes 0289
- Linguistique 0290
- Modernes 0291

Littérature
- Généralités 0401
- Anciennes 0294
- Comparée 0295
- Médiévale 0297
- Moderne 0298
- Africaine 0316
- Américaine 0591
- Anglaise 0593
- Asiatique 0305
- Canadienne (Anglaise) 0352
- Canadienne (Française) 0355
- Germanique 0311
- Latino-américaine 0312
- Moyen-orientale 0315
- Romane 0313
- Slave et est-européenne 0314

PHILOSOPHIE, RELIGION ET THÉOLOGIE

Philosophie 0422
Religion
- Généralités 0318
- Clergé 0319
- Études bibliques 0321
- Histoire des religions 0320
- Philosophie de la religion 0322

Théologie 0469

SCIENCES SOCIALES

Anthropologie
- Archéologie 0324
- Culturelle 0326
- Physique 0327

Droit 0398
Économie
- Généralités 0501
- Commerce-Affaires 0505
- Économie agricole 0503
- Économie du travail 0510
- Finances 0508
- Histoire 0509
- Théorie 0511

Études américaines 0323
Études canadiennes 0385
Études féministes 0453
Folklore 0358
Géographie 0366
Gérontologie 0351
Gestion des affaires
- Généralités 0310
- Administration 0454
- Banques 0770
- Comptabilité 0272
- Marketing 0338

Histoire
- Histoire générale 0578
- Ancienne 0579
- Médiévale 0581
- Moderne 0582
- Histoire des noirs 0328
- Africaine 0331
- Canadienne 0334
- États-Unis 0337
- Européenne 0335
- Moyen-orientale 0333
- Latino-américaine 0336
- Asie, Australie et Océanie 0332

Histoire des sciences 0585
Loisirs 0814
Planification urbaine et régionale 0999
Science politique
- Généralités 0615
- Administration publique 0617
- Droit et relations internationales 0616

Sociologie
- Généralités 0626
- Aide et bien-âtre social 0630
- Criminologie et établissements pénitentiaires 0627
- Démographie 0938
- Études de l' individu et de la famille 0628
- Études des relations interethniques et des relations raciales 0631
- Structure et développement social 0700
- Théorie et méthodes. 0344
- Travail et relations industrielles 0629

Transports 0709
Travail social 0452

SCIENCES ET INGÉNIERIE

SCIENCES BIOLOGIQUES

Agriculture
- Généralités 0473
- Agronomie. 0285
- Alimentation et technologie alimentaire 0359
- Culture 0479
- Élevage et alimentation 0475
- Exploitation des pâturages 0777
- Pathologie animale 0476
- Pathologie végétale 0480
- Physiologie végétale 0817
- Sylviculture et faune 0478
- Technologie du bois 0746

Biologie
- Généralités 0306
- Anatomie 0287
- Biologie (Statistiques) 0308
- Biologie moléculaire 0307
- Botanique 0309
- Cellule 0379
- Écologie 0329
- Entomologie 0353
- Génétique 0369
- Limnologie 0793
- Microbiologie 0410
- Neurologie 0317
- Océanographie 0416
- Physiologie 0433
- Radiation 0821
- Science vétérinaire 0778
- Zoologie 0472

Biophysique
- Généralités 0786
- Medicale 0760

SCIENCES DE LA TERRE

Biogéochimie 0425
Géochimie 0996
Géodésie 0370
Géographie physique 0368
Géologie 0372
Géophysique 0373
Hydrologie 0388
Minéralogie 0411
Océanographie physique 0415
Paléobotanique 0345
Paléoécologie 0426
Paléontologie 0418
Paléozoologie 0985
Palynologie 0427

SCIENCES DE LA SANTÉ ET DE L'ENVIRONNEMENT

Économie domestique 0386
Sciences de l'environnement 0768
Sciences de la santé
- Généralités 0566
- Administration des hôpitaux 0769
- Alimentation et nutrition 0570
- Audiologie 0300
- Chimiothérapie 0992
- Dentisterie 0567
- Développement humain 0758
- Enseignement 0350
- Immunologie 0982
- Loisirs 0575
- Médecine du travail et thérapie 0354
- Médecine et chirurgie 0564
- Obstétrique et gynécologie 0380
- Ophtalmologie 0381
- Orthophonie 0460
- Pathologie 0571
- Pharmacie 0572
- Pharmacologie 0419
- Physiothérapie 0382
- Radiologie 0574
- Santé mentale 0347
- Santé publique 0573
- Soins infirmiers 0569
- Toxicologie 0383

SCIENCES PHYSIQUES

Sciences Pures

Chimie
- Généralités 0485
- Biochimie 487
- Chimie agricole 0749
- Chimie analytique 0486
- Chimie minérale 0488
- Chimie nucléaire 0738
- Chimie organique 0490
- Chimie pharmaceutique 0491
- Physique 0494
- PolymÈres 0495
- Radiation 0754

Mathématiques 0405
Physique
- Généralités 0605
- Acoustique 0986
- Astronomie et astrophysique 0606
- Electronique et électricité 0607
- Fluides et plasma 0759
- Météorologie 0608
- Optique 0752
- Particules (Physique nucléaire) 0798
- Physique atomique 0748
- Physique de l'état solide 0611
- Physique moléculaire 0609
- Physique nucléaire 0610
- Radiation 0756

Statistiques 0463

Sciences Appliqués Et Technologie

Informatique 0984
Ingénierie
- Généralités 0537
- Agricole 0539
- Automobile 0540
- Biomédicale 0541
- Chaleur et thermodynamique 0348
- Conditionnement (Emballage) 0549
- Génie aérospatial 0538
- Génie chimique 0542
- Génie civil 0543
- Génie électronique et électrique 0544
- Génie industriel 0546
- Génie mécanique 0548
- Génie nucléaire 0552
- Ingénierie des systèmes 0790
- Mécanique navale 0547
- Métallurgie 0743
- Science des matériaux 0794
- Technique du pétrole 0765
- Technique minière 0551
- Techniques sanitaires et municipales 0554
- Technologie hydraulique 0545

Mécanique appliquée 0346
Géotechnologie 0428
Matières plastiques (Technologie) 0795
Recherche opérationnelle 0796
Textiles et tissus (Technologie) 0794

PSYCHOLOGIE

Généralités 0621
Personnalité 0625
Psychobiologie 0349
Psychologie clinique 0622
Psychologie du comportement 0384
Psychologie du développement 0620
Psychologie expérimentale 0623
Psychologie industrielle 0624
Psychologie physiologique 0989
Psychologie sociale 0451
Psychométrie 0632

THE UNIVERSITY OF CALGARY

FACULTY OF GRADUATE STUDIES

The undersigned certify that they have read, and recommend to the Faculty of Graduate Studies for acceptance, a thesis entitled "Numerical Solution of Chemical Absorption of H_2S by an Amine - Containing Spray in Plug Flow, With Cumulative Effects" submitted by David Strutt in partial fulfillment of the requirements for the degree of Master of Science in Engineering.

Supervisor, Dr. E. Rhodes
President, Technical University of Nova Scotia

Interim Supervisor, Dr. A. Chakma
Department of Chemical and Petroleum Engineering

Dr. J. Belgrave
Department of Chemical and Petroleum Engineering

Dr. L. Bauwens
Department of Mechanical Engineering

May 4, 1994
Date

ABSTRACT

A model of the chemical absorption of H_2S by an amine containing spray moving in plug flow with the dirty gas is described. The contactor is known as a Waterloo scrubber. The diffusion equations are given, and the spray discretized into a small number of droplet sizes. A Fortran program is presented which solves the finite difference equations and outputs the gas side H_2S concentration against distance travelled. Included in the program is a marching method procedure for iterating reaction front positions under certain conditions. Results show very rapid mass transfer, with variations according to the feed ratio of amine to H_2S. For some values calculations have to be stopped prematurely. A more robust algorithm is recommended, as well as a more realistic model of mass transfer in the gas phase.

ACKNOWLEDGEMENTS

The author would like to thank Dr. E. Rhodes for his helpful suggestions and guidance, and for his patience. Thanks go out also to Dr. D.R. Spink of the University of Waterloo, Waterloo ON for providing very useful information and literature, and also to the University of Calgary for financial support.

TABLE OF CONTENTS

LIST OF TABLES

LIST OF FIGURES

NOMENCLATURE

a	H_2S liquid phase concentration, $kmol/m^3$
A^*	Maximum H_2S liquid phase concentration, $kmol/m^3$
A	Dimensionless H_2S concentration
A_{BULK}	Concentration of H_2S in bulk of gas, $kmol/m^3$
$AREA_1$	Area beneath u curve
$AREA_2$	Area beneath θ curve
b	MEA liquid phase concentration, $kmol/m^3$
B^0	Initial MEA concentration, $kmol/m^3$
B	Dimensionless MEA concentration
D	Droplet diameter, m
D_0	Droplet diameter, m
D_{DROP}	Droplet diameter, m
D_{LIM}	Boundary diameter, m
D_{PEAK}	Peak diameter, m
D_{SM}	Sauter mean diameter, m
D_1	Diffusivity of H_2S in liquid, m^2/s
D_2	Diffusivity of MEA in liquid, m^2/s
D_{PIPE}	Pipe inside diameter, m
e	Base of natural logarithmic function
F	Function to find root of in Newton-Raphson routine
F'	Derivative of F
FLAG	Flag quantity
K	Constant
K_{EQM}	Conversion factor between equilibrium H_2S gas

	and liquid concentrations, dimensionless
L/G	Liquid to gas ratio, U.S. gal/1000 ft^3 gas
M_{RATIO}	Molar feed ratio of MEA to H_2S
N	Rosin-Rammler distribution parameter
N_{DROP}	Number of drops spray is discretized into
N_{IVAL}	Number of intervals the radius of a droplet is subdivided into
p	Fraction of reaction front position
r	Radius, m
R	Droplet radius, m
S	Cumulative surface area distribution, dimensionless
S′	Surface area distribution equation, m^{-1}
Sum	Summation quantity
t	Time, s
u	Dimensionless H_2S concentration in converted coordinate system
V	Cumulative volume distribution, dimensionless
V′	Volume distribution equation, m^{-1}
V_g	Gas velocity, m/s
V_{FL}	Liquid volume fraction in two phase mixture
X	Rosin-Rammler size parameter, m
x	Distance in direction of gas motion, m
y	Independent variable in Newton-Raphson routine
z	Stoichiometric coefficient
z	Inverted dimensionless radius

Greek symbols

α	Reaction front speed factor, m^2/s
$\bar{\alpha}$	Dimensionless α
Δ	Increment
λ	Reaction front depth, m
$\bar{\chi}$	Dimensionless inverted reaction front position
η	Dimensionless radius
θ	Dimensionless MEA concentration in converted coordinate system
τ	Dimensionless time

Subscripts

i	Index of grid line just prior to reaction front
j	Current time level
k, K	Droplet number
l	Counter
n	Generic space index
s	For start of numerical calculations

CHAPTER 1

INTRODUCTION

Gas - liquid mass transfer processes in which the liquid is the dispersed phase occur in a number of different well known devices, including spray dryers and venturi scrubbers. One such device which is a relative youngster is the Waterloo scrubber, developed by D.R. Spink at the University of Waterloo, Ontario Canada. The Waterloo scrubber is a gas-liquid contactor made up of one or more two-phase atomizing nozzles installed in a duct or pipe carrying dirty gas. At the end of the duct is a slowly-turning radial bladed industrial fan, which serves as a turbulent mixing chamber/agglomerator. Very good gas-liquid contact takes place in the device. The unit has been demonstrated to be highly effective in particulate removal operations, as well as for gas absorption. It has numerous other advantages which make it an attractive option for such applications (Spink, D.R., 1988). Figure 1 shows a view of a Waterloo scrubber.

As such, the question has arisen if the Waterloo scrubber might find use in H_2S removal from sour gas by amines. If so, then a theoretically based model of the mass transfer occuring in the device would be of great value in designing units for particular uses.

In this thesis attempts at modelling chemical absorption of H_2S by an amine solution in a Waterloo scrubber are

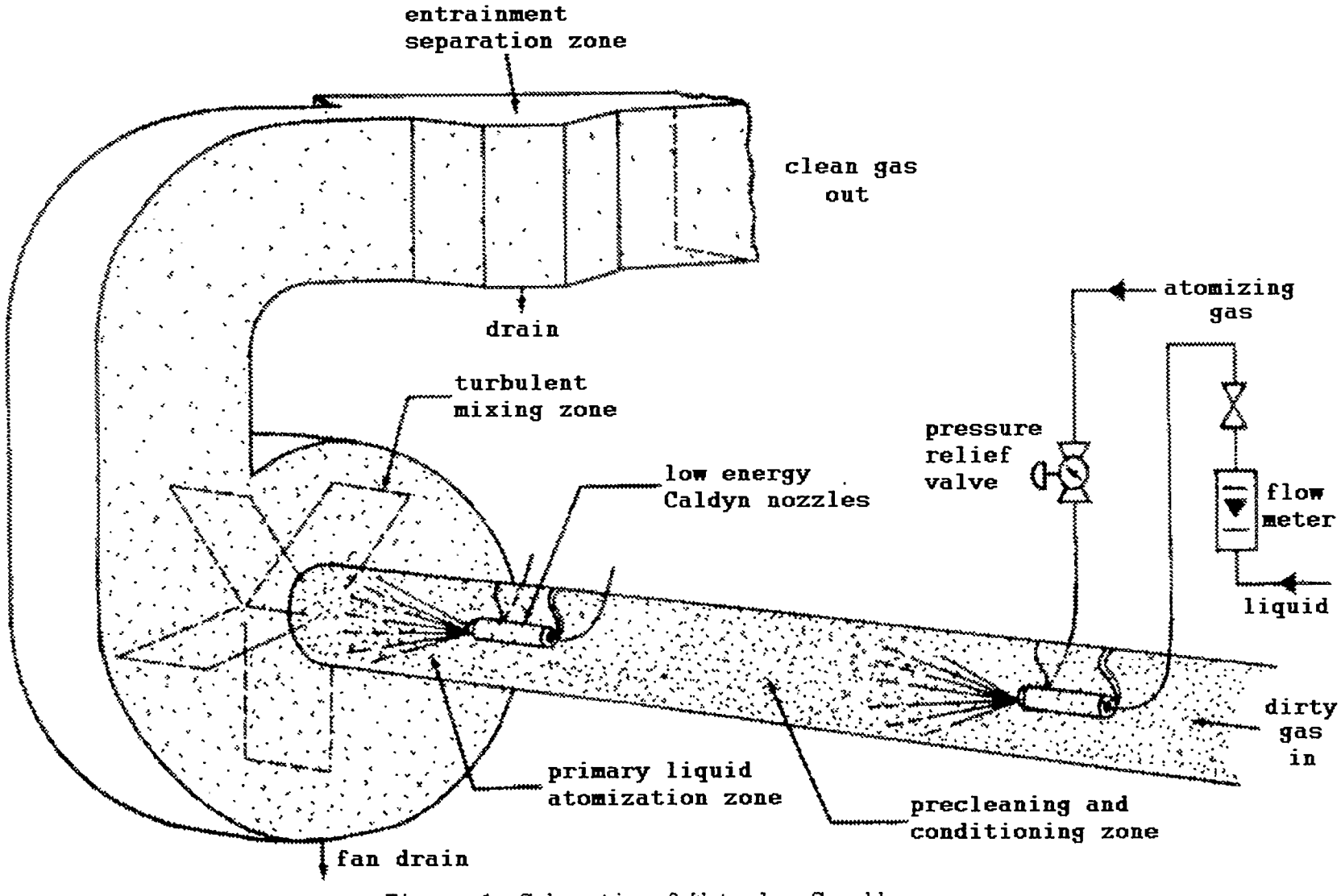

Figure 1: Schematic of Waterloo Scrubber

presented. The model is outlined and expressed mathematically, and then the appropriate substitutions and simplifications are made to permit solution. A computer program to solve the model is presented, and results for a number of trial runs are given. Appropriate discussion is then made, and recommendations given.

CHAPTER 2

LITERATURE REVIEW

No papers were found which deal with the modelling of gas - liquid mass transfer in sprays on the single droplet level. Related papers found include the well known work of Ranz and Marshall (1952) in which mass and heat transfer from single droplets is examined. A handy expression for the Nusselt number is given, but the Reynolds numbers range of its applicability is quite small (Ranz and Marshall, 1952). The paper of Elghobashi, et al. (1981) presents results from experimental measurements of point concentrations of a tracer injected into a gas stream in a countercurrent jet. However, the geometry of their system is the reverse of that here.

In terms of modelling what goes on inside the droplets, a number of relevant references were discovered. Danckwerts (1970) gives the solution of the analogous problem in rectangular coordinates, which is very useful. In spherical coordinates, there is the paper of Dursunkaya and Nair (1990), the numerous papers of Dewynne and Hill (1984, 1985, 1986), and others (Chuang and Szekely, 1971; Pedroso and Domoto, 1973; Riley, et al., 1974; Soward, 1980; Voller and Cross, 1981). At this point however a full discussion of these papers would not be appropriate; the papers will be described at the beginning of chapter 4, in relation to their usefulness in attempts at finding an analytical solution to the problem.

CHAPTER 3

MODEL

3.1 Introduction

In modelling the mass transfer that occurs there, the Waterloo scrubber can be viewed as being comprised of two sections: 1. an initial region where the two phase jet is expanding into the dirty gas stream, entraining the surrounding gas and undergoing momentum transfer, and 2. a region in which the jet and the dirty gas have completely mixed and are at the same velocity. The exact position of the boundary between the two regions relative to the nozzle orifice would be a function of the spray velocity and angle, and the dirty gas flowrate, as well as other system parameters. Modelling the first section of the scrubber would seem to be extremely difficult, requiring specific knowledge of the behaviour of the chosen nozzle, velocity distributions across the jet cross-section, and details of how the gas stream and jet mix. Some such information is available (Levich, 1962; Perry, 1984, pg 5-22; Lukashev, 1988) but the relations are for single phase jets at low pressures spraying into stagnant atmospheres. As such, this study will only go so far as to model the second section of the scrubber. It can be presumed however that most of the mass transfer occurs in this section, as in the first section the mixing of the jet and dirty gas is incomplete, so the droplets of scrubbing liquid

are not exposed to the complete gradient of H_2S.

3.2 Modelling

What is desired from the model of the second section of the scrubber is the bulk concentration of H_2S in the gas phase along its path in the duct. This would allow simple determination of the length of pipe needed to achieve a desired exit concentration. In modelling the scrubber, on the macroscopic level the droplet size distribution in the spray must be known, to permit discretization into a finite number of droplet sizes. Then the mass transfer equations must be solved for each droplet size, and finally an overall H_2S mass balance must be performed on the spray to recalculate the H_2S concentration in the gas phase.

3.2.1 Assumptions and Parameters

The second section of the scrubber is assumed to be characterized as follows:

1. The two phase mixture in the duct is in plug flow at a constant velocity, i.e. there are no axial velocity gradients.
2. There is perfect radial mixing (thus there is no gas side resistance to mass transfer).
3. Liquid droplets are rigid spheres, i.e. there are no surface disturbances or internal flow in the droplets (thus mass transfer within the liquid phase occurs by molecular

diffusion only). This can be justified by considering the large viscosity ratio between the gas and liquid phases, on the order of 100.

4. Only H_2S is being absorbed from the gas. Thus the gas stream cannot contain CO_2, unless the amine used is one which selectively absorbs H_2S over CO_2, for example TEA or MDEA (Danckwerts and Sharma, 1966, pg. 267).
5. Isothermal operation.
6. Physical properties are constant (thus the amine concentration in the liquid is fairly low, so the amount of H_2S absorbed is never enough to significantly change the liquid properties).
7. Flowrates are small, i.e. convective effects can be neglected.
8. Equilibrium exists at all times across the gas-liquid interface.

The specific amine considered for this project is monoethanolamine ("MEA", $HO\text{-}CH_2\text{-}CH_2\text{-}NH_2$), which reacts instantaneously with H_2S in a 1 - 1 molar ratio:

$$HOCH_2CH_2NH_{2(aq)} + H_2S_{(aq)} \rightarrow HOCH_2CH_2NH_3^+{}_{(aq)} + HS^-{}_{(aq)} \qquad (1)$$

(Swaddle, 1986, pg. 59). The reaction between these two species is known to be very fast, and so here it is assumed instantaneous (Danckwerts and Sharma, 1966, pg. 267). The chemical reaction in the liquid is instantaneous and irreversible (corresponding to low temperature and high pressure conditions). As a result of the assumptions the

process can be viewed as liquid phase mass transfer limited. Hence the gas phase can be ignored, and only the mass transfer within the liquid phase must be calculated.

The system parameters which must be specified in order to completely define the problem are as follows:

- diffusivities of both species in the liquid phase
- ratio of maximum liquid phase concentrations of both species
- ratio of total molar feed flowrates of the species in the two phase mixture
- linear velocity of the two phase mixture in the duct

3.2.2 Moving Boundary Problem

Because of the instantaneous reaction which occurs between H_2S and MEA, inside each droplet will exist two distinct regions of concentration. In each region only one of the two species can exist unreacted. Where the two regions meet is the moving front at which the reaction occurs. Here the concentrations of both species are zero. The front moves inwards towards the droplet centre as the amine is depleted. The reaction at the front occurs at a rate equal to the rate the two reactants can diffuse to it. Problems of this type in which there is a moving surface are known as moving boundary problems.

As more and more H_2S is absorbed into the droplets, its bulk concentration in the gas phase will drop. Thus the

equilibrium liquid concentration at the surface of each droplet will also decrease. This gives a time dependent boundary condition at the surface. In spherical coordinates, the problem reduces to the simultaneous diffusion of H_2S (the chemical solute) and MEA (the chemical solvent) to a reaction front, followed by instantaneous chemical reaction. The solution consists of concentration profiles of both species across their appropriate regions of the droplet over time, as well as the position of the moving reaction front against time.

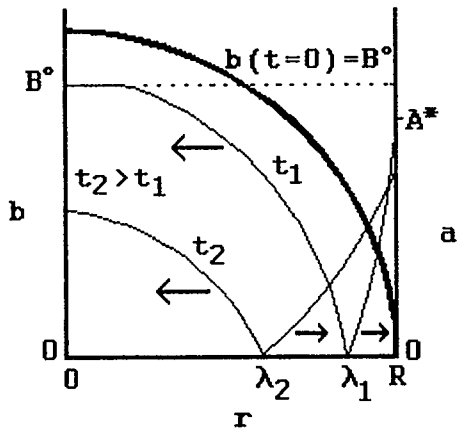

Figure 2: Diagram of Droplet

Figure 2 shows an internal view of a liquid droplet, highlighting all the variables used. λ is the position of the reaction front at time t. The equations to be solved are the diffusion equation in spherical coordinates for both the reactants (see the Nomenclature for descriptions of each quantity with units):

$$\frac{D_1}{r^2}\frac{\partial}{\partial r}\left(r^2\frac{\partial a}{\partial r}\right) = \frac{\partial a}{\partial t} \quad \lambda(t) \le r \le R; \quad \begin{matrix} r=R, a=a(R,t), t>0 \\ [a(R,0)=A^*] \\ r=\lambda(t), a=0, t>0 \end{matrix} \qquad (2)$$

$$\frac{D_2}{r^2}\frac{\partial}{\partial r}\left(r^2\frac{\partial b}{\partial r}\right) = \frac{\partial b}{\partial t} \quad 0\le r\le\lambda(t); \quad \begin{matrix} t=0, b=B^0, 0\le r<R \\ r=\lambda(t), b=0, t>0 \\ r=0, \frac{\partial b}{\partial r}=0, t>0 \end{matrix} \qquad (3)$$

The first boundary condition for equation 2 expresses that the surface concentration of the absorbed H_2S is specified each time step to be in equilibrium with the amount remaining in the gas phase. The original value of A^* is the concentration that would be in equilibrium with the H_2S in the inlet gas. There is no initial condition for H_2S, as initially it is not present in the liquid phase. The initial condition for MEA is a flat profile of its initial concentration. The second boundary condition for equation 2 is that of symmetry around the centre of the droplet.

An additional equation is written at λ, the position of the reaction front, to express the reaction stoichiometry:

$$-zD_1\frac{\partial a}{\partial r}\Big|_\lambda = D_2\frac{\partial b}{\partial r}\Big|_\lambda \quad t>0;\ t=0, \lambda=R \qquad (4)$$

That is, the fluxes of the two species at the position of the moving front are stoichiometrically equal. For the system H_2S - MEA, z is 1. This condition is referred to as a Stefan condition, in honour of J. Stefan, pioneer of moving boundary problems in the late 19th century (Crank, 1984, pg. 2). The consequence of this condition is that both equations 2 and 3 must be solved simultaneously. The complete solution is then:

$$\begin{matrix} a(r, t), & \lambda(t)\le r\le R \\ b(r, t), & 0\le r\le\lambda(t) \\ \lambda(t), & t>0 \end{matrix} \qquad (5)$$

This problem is the spherical equivalent of the classic diffusion moving boundary problem presented by Danckwerts (Danckwerts, 1970). This problem has a well known analytical solution and as such is very useful in the solving of this problem (see Appendix A for the solution).

3.2.3 Spray Discretization

In the true spray there exists an extremely large number of droplet sizes, a different one for each droplet. At every cross-section of the spray, the droplets all have different concentration profiles from each other, with those in the smaller droplets being more advanced than in the larger ones. In practice of course only a finite number of droplet sizes can be solved for. Thus it is necessary to replace the original continuous distribution of droplet diameters with a discrete distribution of only a few diameters. The diameters should be chosen in such a way that the discrete distribution has the same total surface area as the true spray.

In order to do this, the droplet size distribution in the spray must be represented by a statistical model. Following the example of a report from the University of Waterloo on the measurement of droplet size distributions from the nozzles commercially used in Waterloo scrubbers (Brena de la Rosa, 1987), the spray model chosen is the Rosin-Rammler distribution. This droplet size distribution is used in the report as it gives a very good curve fit to the measured data

(Brena de la Rosa, 1987, pg. 4).

The Rosin-Rammler droplet size distribution function is a two parameter model, usually given in the cumulative volume form:

$$V=1-e^{-(D/X)^N} \qquad (6)$$

Here V is the volume fraction of the spray occuring in drops of diameters less than D meters, X is the size parameter (in meters), N is the distribution parameter, and e is the base of the natural logarithmic function. The basis for subdividing the spray is that each droplet size should represent an equal fraction of the total surface area of the spray. As such, it is necessary to first obtain a cumulative surface area distribution from equation 6. Depending on the number of droplet sizes the spray is to be discretized into, this equation would give the boundary diameters between which the appropriate fraction of the total surface area of the spray is held. In the intervals between each of these boundary diameters a Sauter mean diameter could be found. This last step would require a surface area distribution equation. Thus from the initial Rosin-Rammler droplet size distribution equation, both a cumulative surface area distribution and a surface area distribution equation must be derived.

The surface area distribution equation is a function which when integrated between two diameters gives the fraction of the total surface area of the spray occuring in droplets between those diameters. It is computed from the Rosin-Rammler

volume distribution equation as such:

$$S'(D) = \frac{K}{D} V'(D) \tag{7}$$

Here S'(D) is the surface area distribution equation, V'(D) is the volume distribution equation, and K is a constant which makes the area beneath S'(D) from 0 to ∞ equal to 1. The volume distribution equation V'(D) is the derivative of equation 6:

$$V'(D) = \frac{dV}{dD} = \frac{ND^{N-1}}{X^N} e^{-(D/X)^N} \tag{8}$$

Integrating the resulting equation from 0 to ∞ to solve for K, and substituting back gives as a final result:

$$S'(D) = \frac{N}{\Gamma(1-\frac{1}{N})} \frac{D^{N-2}}{X^{N-1}} e^{-(D/X)^N} \tag{9}$$

The cumulative surface area distribution is derived by integrating equation 9:

$$S(D_0) = \int_0^{D_0} S'(D)\, dD = P\left(1-\frac{1}{N}, \left(\frac{D_0}{X}\right)^N\right) \tag{10}$$

The cumulative distribution is S, and D_0 is a certain diameter. The result is the incomplete gamma function, represented by P.

3.2.4 Mass Balance

The entire point of any mass transfer process such as the one being considered is that the bulk concentration of a component of the gas phase be reduced as the gas travels along

the length of the contacting device. In this case, as the droplets move along the duct, more and more H_2S is absorbed into each, shifting the concentration profiles towards the centre of the droplets. Hence to compute the H_2S concentration along the duct, the amount absorbed into each droplet size must be calculated, and then the results extrapolated across the entire spray.

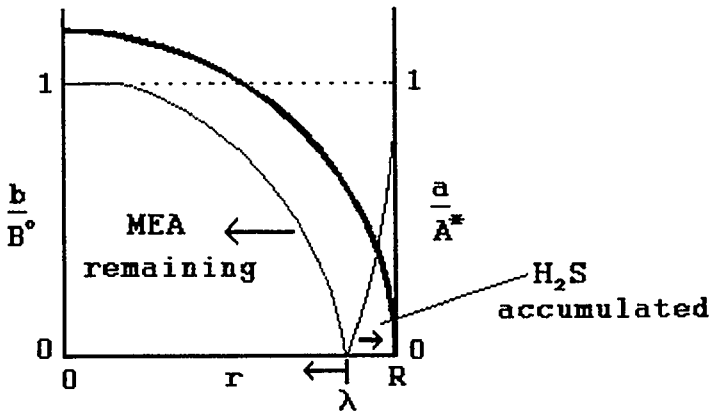

Figure 3: Concentration Regions in Sphere

Figure 3 shows again a view of the concentration profiles inside a liquid droplet, similar to Figure 2. To compute the amount of H_2S absorbed by the droplet, the areas beneath the curves must be computed. A straightforward mass balance is performed (units are mol/drop):

$$\begin{aligned}(H_2S \text{ absorbed}) &= (H_2S \text{ accumulated}) + (H_2S \text{ consumed}) \\ &= (H_2S \text{ accumulated}) + z * (\text{MEA consumed}) \\ &= (H_2S \text{ accumulated}) + [(\text{MEA originally}) - (\text{MEA remaining})]\end{aligned} \quad (11)$$

The amount of H_2S accumulated is the area beneath the H_2S curve in Figure 3, and the amount of MEA remaining is the area beneath the MEA curve. The original amount of MEA in the liquid is its feed concentration times the droplet volume.

Hence:

$$(H_2S \text{ absorbed}) = \int_{\lambda(t)}^{R} a(r)\,4\pi r^2 dr + B^0 \frac{4}{3}\pi R^3 - \int_{0}^{\lambda(t)} b(r)\,4\pi r^2 dr \qquad (12)$$

An overall H_2S mass balance can then be performed to find the new value of the surface concentration. The total amount of H_2S in a disc shaped section of the duct is calculated as the original amount in the same section when it entered the duct, less the sum of the amount absorbed into each droplet size, weighted by the volume fraction of each. The detailed derivation of this equation is given in the next chapter.

CHAPTER 4

SOLUTION OF MODEL EQUATIONS

4.1 Introduction

The equations which define the model have been given in the previous chapter. This chapter deals with how these equations are solved for a given set of system parameters. As mentioned previously, the desired solution is the gas phase bulk H_2S concentration profile along the length of the contactor. To solve the problem, the partial differential equations (PDEs) must be discretized into finite difference equations, initial profiles must be formulated, and the complete mass balance equation must be derived.

4.2 Solving the Differential Equations

4.2.1 Attempts at Finding an Analytical Solution

Attempts were made at finding an analytical solution to the diffusion equations with no success. All conventional partial differential equation solution procedures are frustrated by the Stefan condition. A search of relevant literature revealed that such a solution is not known. The majority of the literature deals with the analogous heat transfer problem, that of solidification or melting of a sphere. Most papers, however, deal with the simpler single phase version of the problem, in which one of the two phases

is eliminated by considering the temperature profile to be flat (Chuang and Szekely 1971; Hill and Dewynne, 1984; Pedroso and Domoto, 1973; Riley, et al., 1974; Soward, 1980). One of the papers of Dewynne and Hill (1986) deals with the two phase problem in which there are temperature distributions in both solid and liquid phases, but unfortunately they are only able to generate equations for upper and lower bounds on the position of the moving boundary. Even these results are not applicable to this problem however, as they are only accurate for systems in which the heat of fusion is large. The problem of absorption with instantaneous chemical reaction happens to be a special case of the problem of freezing or melting of a sphere, with a heat of fusion of zero. Also because of this, the most commonly used method of numerical solution of these problems, called the enthalpy method, breaks down and is hence useless (Voller and Cross, 1981). A final more recent paper presents a semi-analytical method of solving the problem of freezing of a finite slab, and hints at possible extension to spherical coordinates. However, the method involves repeated calculations of large Fourier series for every grid point, and would take much longer to compute than a finite difference solution (Dursunkaya and Nair, 1990).

4.2.2 Finite Difference Equations

Hence only a numerical solution to the differential equations is possible. Being a problem of straightforward

partial differential equations, a finite difference solution procedure is employed.

4.2.2.1 Changes of Variables

First though, three sets of substitutions are made to convert the equations to a form more suitable for discretization into finite difference formulae. The first change of variables nondimensionalizes the equations:

Substitute

$$\left.\begin{aligned} A&=\frac{a}{A^*}\\ \eta&=\frac{r}{R}\\ \tau&=\frac{D_2 t}{R^2}\end{aligned}\right\} \Rightarrow \quad \frac{D_1}{D_2}\frac{1}{\eta^2}\frac{\partial}{\partial\eta}\left(\eta^2\frac{\partial A}{\partial\eta}\right)=\frac{\partial A}{\partial\tau} \qquad \frac{\lambda(\tau)}{R}\le\eta\le 1$$

$$\eta=1, A=A(1,\tau), \tau>0 \quad [A(1,0)=1]; \quad \eta=\frac{\lambda(\tau)}{R}, A=0, \tau>0 \tag{13}$$

$$B=\frac{b}{B^0} \quad \Rightarrow \quad \frac{1}{\eta^2}\frac{\partial}{\partial\eta}\left(\eta^2\frac{\partial B}{\partial\eta}\right)=\frac{\partial B}{\partial\tau} \qquad 0\le\eta\le\frac{\lambda(\tau)}{R}$$

$$\tau=0, B=1, 0\le\eta<1; \quad \eta=\frac{\lambda(\tau)}{R}, B=0, \tau>0 \quad \eta=0, B=finite, \tau>0 \tag{14}$$

$$-\frac{D_1}{D_2}\frac{\partial A}{\partial\eta}\Big|_{\lambda/R}=\frac{B^0}{A^*}\frac{\partial B}{\partial\eta}\Big|_{\lambda/R} \qquad \tau>0;\ \tau=0, \frac{\lambda}{R}=1 \tag{15}$$

The second change of variables is the standard substitution for reducing spherical coordinate problems to rectangular coordinates:

Substitute

$$u=A\eta \quad \Rightarrow \quad \frac{D_1}{D_2}\frac{\partial^2 u}{\partial\eta^2}=\frac{\partial u}{\partial\tau} \qquad \frac{\lambda(\tau)}{R}\le\eta\le 1; \quad \eta=1, u=u(1,\tau), \tau>0 \quad [u(1,0)=1] \quad \eta=\frac{\lambda(\tau)}{R}, u=0, \tau>0 \tag{16}$$

$$\theta=B\eta \quad \Rightarrow \quad \frac{\partial^2\theta}{\partial\eta^2}=\frac{\partial\theta}{\partial\tau} \qquad 0\le\eta\le\frac{\lambda(\tau)}{R}; \quad \tau=0, \theta=\eta, 0\le\eta<1 \quad \eta=\frac{\lambda(\tau)}{R}, \theta=0, \tau>0 \quad \eta=0, \theta=0, \tau>0 \tag{17}$$

$$-\frac{D_1}{D_2}\frac{\partial u}{\partial \eta}\Big|_{\lambda/R}=\frac{B^0}{A^*}\frac{\partial \theta}{\partial \eta}\Big|_{\lambda/R} \quad \tau>0;\ \tau=0,\ \frac{\lambda}{R}=1 \tag{18}$$

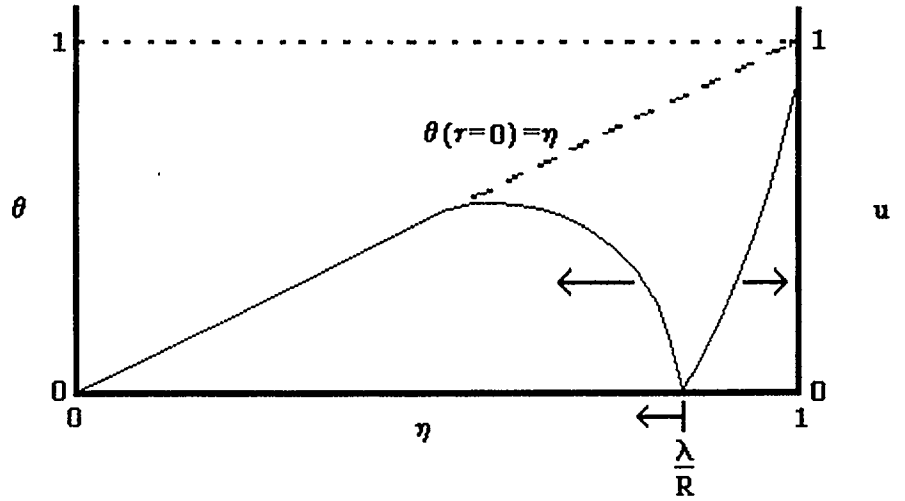

Figure 4: Diagram of Variables for Equations 16 - 18

Figure 4 illustrates the concentration profiles in the new coordinate system created by the last substitution. Equation 18 is derived from equation 4, and is reduced due to the values of u and θ at the reaction front being zero. Of significance here is that for the solvent, the previously flat initial concentration profile in the droplet has been transformed into a straight line, and the symmetry condition at the centre is now a Dirichlet condition, with the value fixed at zero.

One final substitution in the space variable is made to flip the whole system around (here $\hat{\lambda}(\tau) = 1 - \lambda(\tau)/R$):

Substitute

$$z=1-\eta \quad \Rightarrow \quad \frac{D_1}{D_2}\frac{\partial^2 u}{\partial z^2}=\frac{\partial u}{\partial \tau} \quad 0<z\le\hat{\lambda}(\tau);\ \begin{matrix} z=0,\ u=u(0,\tau),\ \tau>0 \\ [u(0,0)=1] \\ z=\hat{\lambda}(\tau),\ u=0,\ \tau>0 \end{matrix} \tag{19}$$

$$z=1-\eta \quad \Rightarrow \quad \frac{\partial^2\theta}{\partial z^2}=\frac{\partial\theta}{\partial\tau} \qquad \bar{\lambda}(\tau)\le z\le 1; \quad \begin{matrix}\tau=0,\theta=1-z,0<z\le 1\\ z=\bar{\lambda}(\tau),\theta=0,\tau>0\\ z=1,\theta=0,\tau>0\end{matrix} \tag{20}$$

$$-\frac{D_1}{D_2}\frac{\partial u}{\partial z}\Big|_{\bar{\lambda}}=\frac{B^0}{A^*}\frac{\partial\theta}{\partial z}\Big|_{\bar{\lambda}} \qquad \tau>0;\ \tau=0,\bar{\lambda}=0 \tag{21}$$

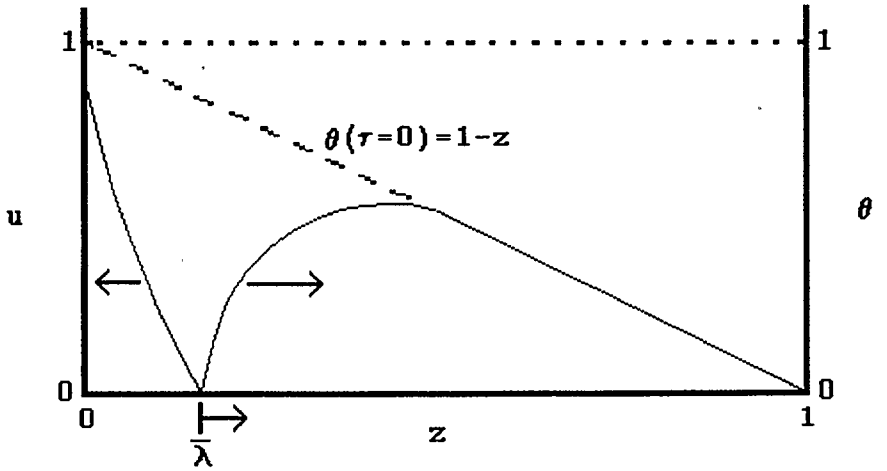

Figure 5: Diagram of Variables for Equations 19 and 20

Figure 5 illustrates the coordinate system for the last three equations. The reason this substitution is made is to convert the problem into one resembling Danckwert's semi-infinite problem as much as possible. Comparing the equations to those in Appendix A, it can be seen that they are identical. The only differences in formulation between the problems are in the initial condition and the inside boundary condition for the chemical solvent. The difference in the initial conditions is that for Danckwert's problem it is a flat line, and for this problem it is a straight line starting at 1 and dropping to 0 at z = 1. The difference between the boundary conditions is simply a reflection of the different geometries of the problems - Danckwert's problem is for a semi-infinite fluid,

while this problem is for a finite environment. The major consequence of the similarity between the problems is that the finite difference equations will be identical for both. This allows easy verification of the validity of the program which solves these equations - a few small changes are all that are necessary to have the program calculate solutions to the Danckwerts problem, which can then be checked against analytical results.

4.2.2.2 Discretization of PDEs

The method used to reduce the partial differential equations 19 and 20 to finite difference equations is an explicit method, with a fixed finite difference grid. Explicit methods were chosen due to ease of use. The PDEs are parabolic, so the approach is well known. Figure 6 shows a diagram of the finite difference grid for a droplet.

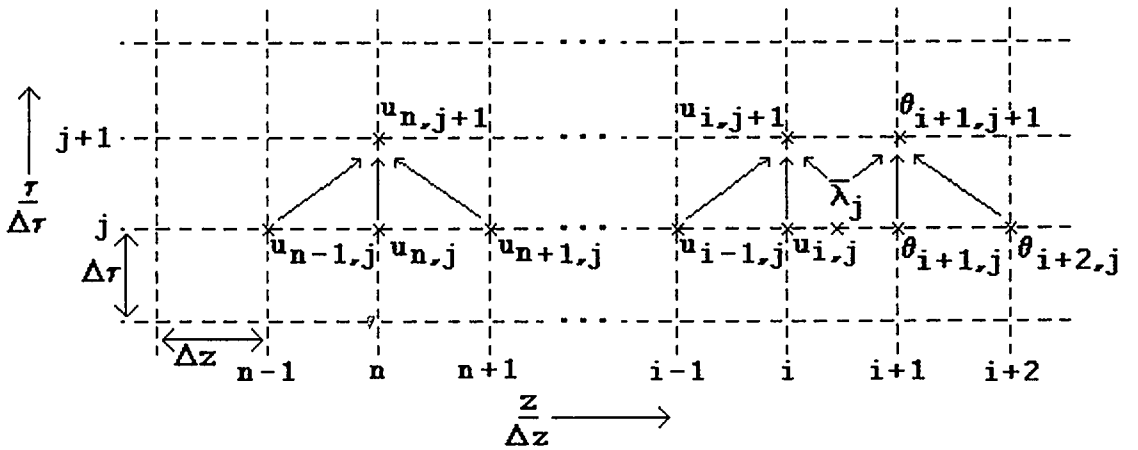

Figure 6: Finite Difference Grid

For each droplet size, the grid widths $\Delta\tau$ and Δz are different. In the diagram, j is the index of the known time

level, and j+1 the index of the unknown time level, for which concentrations are being computed. The index n is the space index of a generic point. Index i in the figure is the index of the space grid line which the reaction front position ($\hat{x}_j$) falls just after.

Figure 6 indicates the customary explicit method interrelationship of points. In this method of discretization, the three closest points from the time level j are used to compute each value for the concentration at the new time level j+1. The appropriate substitutions for equation 19 are as follows:

$$\frac{\partial^2 u}{\partial z^2} \approx \frac{u_{n-1,j} - 2u_{n,j} + u_{n+1,j}}{(\Delta z)^2} \qquad (22)$$
$$\frac{\partial u}{\partial \tau} \approx \frac{u_{n,j+1} - u_{n,j}}{\Delta \tau}$$

The first expression is the second order correct approximation to the second derivative, and the second expression is a first order correct backwards difference approximation to the dimensionless time derivative. Substituting these into equation 19 and solving for the unknown at the new time step:

$$u_{n,j+1} = u_{n,j} + \frac{(D_1/D_2)\Delta\tau}{(\Delta z)^2}(u_{n+1,j} - 2u_{n,j} + u_{n-1,j}) \quad n=1,2,\ldots,i-1 \qquad (23)$$

Thus using this equation the new value of H_2S concentration for each grid point between the surface and the point prior to the reaction front position is computed easily in a loop. The boundary conditions become:

$$u_{0,j} = u(0) \qquad (24)$$
$$u_{i+p_j,j} = 0$$

The stability criterion for equation 23 is:

$$\Delta\tau \leq \frac{(\Delta z)^2}{2\,(D_1/D_2)} \tag{25}$$

A similar procedure is followed to discretize equation 20. First the finite difference approximations to the derivatives:

$$\frac{\partial^2\theta}{\partial z^2} \approx \frac{\theta_{n-1,j}-2\theta_{n,j}+\theta_{n+1,j}}{(\Delta z)^2}$$
$$\frac{\partial\theta}{\partial\tau} \approx \frac{\theta_{n,j+1}-\theta_{n,j}}{\Delta\tau} \tag{26}$$

Substituting this into equation 20 and solving for the single unknown:

$$\theta_{n,j+1}=\theta_{n,j}+\frac{\Delta\tau}{(\Delta z)^2}\,(\theta_{n+1,j}-2\theta_{n,j}+\theta_{n-1,j}) \qquad n=i+2,\,i+3,\,\ldots,\,N_{ival}-1 \tag{27}$$

New values of the MEA concentration are calculated using this from one grid point after that which follows the reaction front to the last point prior to the droplet centre, or z = 1. The initial conditions and boundary conditions:

$$\theta_{n,0}=1-n(\Delta z),\ n=0,1,2,\ldots$$
$$\theta_{N_{IVAL},j}=0 \tag{28}$$
$$\theta_{i+p_j,j}=0$$

The stability criterion for this equation is:

$$\Delta\tau \leq \frac{(\Delta z)^2}{2} \tag{29}$$

The value of $\Delta\tau$ chosen for calculations is half the smaller of the two values given by equations 25 and 29.

The two points surrounding the reaction front $u_{i,j+1}$ and $\theta_{i+1,j+1}$ are handled differently than the other points. As

before, the concentrations are calculated from the three closest points from the previous time step. However, in each case one of the points is the reaction front. This is illustrated in Figure 6. Thus the problem arises that the points are not evenly spaced. This problem is dealt with by representing each curve in the vicinity of the reaction front by a three-point Lagrangian interpolatory polynomial. For the H_2S curve, the polynomial passes through the points $u_{i-1,j}$, $u_{i,j}$, and $u_{i+pj,j}$. For the MEA curve, the polynomial passes through $\theta_{i+pj,j}$, $\theta_{i+1,j}$, and $\theta_{i+2,j}$. From the interpolatory polynomials, formulae for the second space derivatives can be derived for the two positions of interest, and then substituted back into the original differential equations along with the same approximation for the time derivative as before. From Crank (1984, pg. 165), the second derivative approximations are:

$$\frac{\partial^2 u}{\partial z^2} \approx \frac{2}{(\Delta z)^2}\left(\frac{u_{i-1,j}}{p_j+1} - \frac{u_{i,j}}{p_j}\right) \qquad z=i\Delta z \tag{30}$$

$$\frac{\partial^2 \theta}{\partial z^2} \approx \frac{2}{(\Delta z)^2}\left(-\frac{\theta_{i+1,j}}{1-p_j} + \frac{\theta_{i+2,j}}{2-p_j}\right) \qquad z=(i+1)\Delta z \tag{31}$$

Substituting these into equations 19 and 20 respectively, along with backwards differences in time, yields the finite difference formulae for the two points surrounding the reaction front:

$$u_{i,j+1} = u_{i,j} + \frac{2(D_1/D_2)\Delta\tau}{(\Delta z)^2}\left(\frac{u_{i-1,j}}{p_j+1} - \frac{u_{i,j}}{p_j}\right) \tag{32}$$

$$\theta_{i+1,j+1}=\theta_{i+1,j}-\frac{2\Delta\tau}{(\Delta z)^2}\left(\frac{\theta_{i+1,j}}{1-p_j}-\frac{\theta_{i+2,j}}{2-p_j}\right) \qquad (33)$$

Thus using equations 23, 27, 32 and 33, the complete concentration profiles for both H_2S and MEA are computed for the new time level j+1. The updated position of the reaction front p_{j+1} has next to be found. Starting from the newly computed profile, the value is computed so as to satisfy the Stefan condition, equation 21. Here the interpolatory polynomial idea is employed again, to find formulae for the first space derivatives of the two concentration curves at the reaction front position for the new time level. From Crank (1984, pg. 165), the formulae are:

$$\frac{\partial u}{\partial z}\approx\frac{1}{\Delta z}\left(\frac{p_{j+1}u_{i-1,j+1}}{p_{j+1}+1}-\frac{(p_{j+1}+1)\,u_{i,j+1}}{p_{j+1}}\right) \quad z=(i+p_{j+1})\,\Delta z \qquad (34)$$

$$\frac{\partial \theta}{\partial z}\approx\frac{1}{\Delta z}\left(\frac{2-p_{j+1}}{1-p_{j+1}}\theta_{i+1,j+1}-\frac{1-p_{j+1}}{2-p_{j+1}}\theta_{i+2,j+1}\right) \quad z=(i+p_{j+1})\,\Delta z \qquad (35)$$

Putting these into equation 21 and simplifying gives:

$$\frac{(p_{j+1}+1)\,u_{i,j+1}}{p_{j+1}}-\frac{p_{j+1}u_{i-1,j+1}}{p_{j+1}+1}=\frac{B^0/A^*}{D_1/D_2}\left(\frac{2-p_{j+1}}{1-p_{j+1}}\theta_{i+1,j+1}-\frac{1-p_{j+1}}{2-p_{j+1}}\theta_{i+2,j+1}\right) \qquad (36)$$

This is one equation in the one unknown p_{j+1}, which can be solved by a nonlinear equation solving routine.

As the calculations proceed, at various times the reaction front in each droplet will approach a grid line, i.e. p_{j+1} will become close to 1. This creates a problem, as according to equation 36, as $p_{j+1} \rightarrow 1$, the denominator of the first term on the right hand side goes to zero. To avoid this difficulty, a marching numerical technique is employed for the

calculation of the reaction front positions. Once p_{j+1} has come within a certain range of 1, the use of equation 36 is suspended, and for the consequent time steps p_{j+1} is incremented by the amount it changed in the previous use of equation 36. This marching procedure is continued past unity (at which the value is reset by subtracting 1) until an equal distance beyond 1 is passed. Equation 36 is then 'turned back on'. During the marching procedure, when p_{j+1} remains less than 1, equation 33 is not used due to the denominator term 1 - p_j, which gives unstable results in this region. Similarly, once the reaction front has passed the grid line and p_{j+1} is near zero, equation 32 is not used due to the p_j denominator term. In each case, the respective term is held at zero.

4.2.3 Initial Profiles

To begin the finite difference calculations the reaction front must have passed at least one grid point. This is the minimum initial level of development of the H_2S profile in the liquid. At this level, the entire u profile consists of only three points, $u_{0,j}$, $u_{1,j}$, and $u_{1+pj,j}$. To find a suitable starting profile, an analogy is drawn between the problem of mass transfer to a sphere and that of mass transfer to a semi-infinite slab, i.e. Danckwerts' problem. At small times, the depth of penetration of the reaction front into the droplet will be very small compared to its diameter, and the drawdown of the MEA concentration profile from its initial level will

not extend very far. As such the droplet can effectively be viewed as infinitely deep. Also, with the reaction front being so close to the surface of the droplet, the concavity of the droplet can be neglected, and so the droplet can be considered as a slab. Therefore initially the concentration profiles in the droplet will be the same as those in a semi-infinite slab. The solution to Danckwerts' problem can then be used to find the initial profiles in the droplets.

In the solution to Danckwerts' problem given in Appendix A, the length x represents distance from the gas-liquid interface. The corresponding quantity in spherical coordinates is R - r. With this substitution made, the initial profiles in the sphere are:

$$\frac{a}{A^*}=1-\frac{erf\left(\frac{R-r}{2\sqrt{D_1 t_s}}\right)}{erf\sqrt{\frac{\alpha}{D_1}}} \qquad \lambda_s \le r \le R \tag{37}$$

$$\frac{b}{B^0}=1-\frac{erfc\left(\frac{R-r}{2\sqrt{D_2 t_s}}\right)}{erfc\sqrt{\frac{\alpha}{D_2}}} \qquad 0 \le r \le \lambda_s \tag{38}$$

Here λ_s is the reaction front position (for the start of numerical calculations) and t_s the corresponding time. The value of λ_s is the same for all droplet sizes. In practise λ_s is specified and t_s calculated by:

$$R-\lambda_s=2\sqrt{\alpha t_s} \Rightarrow t_s=\frac{(R-\lambda_s)^2}{4\alpha} \tag{39}$$

The quantity α is a system parameter calculated from the

initial concentrations and component diffusivities. The formula is the same as for the semi-infinite problem (see Appendix A for derivation):

$$e^{\alpha\left(\frac{1}{D_2}-\frac{1}{D_1}\right)}\frac{erfc\sqrt{\frac{\alpha}{D_2}}}{erf\sqrt{\frac{\alpha}{D_1}}}=\frac{B^0/A^*}{\sqrt{D_1/D_2}} \tag{40}$$

Of course as outlined above the problem actually being solved uses dimensionless variables in a modified coordinate system. Therefore the initial profiles must be converted to the same variables for use. To nondimensionalize:

$$\left.\begin{array}{l}\textit{Substitute}\\ A=\frac{a}{A^*}\\ \eta=\frac{r}{R}\\ \tau_s=\frac{D_2 t_s}{R^2}\\ \bar{\alpha}=\frac{\alpha}{D_2}\end{array}\right\} \Rightarrow A=1-\frac{erf\left(\frac{1-\eta}{2\sqrt{\tau_s D_1/D_2}}\right)}{erf\sqrt{\frac{\bar{\alpha}}{D_1/D_2}}} \qquad \frac{\lambda_s}{R}\le\eta\le 1 \tag{41}$$

$$B=\frac{b}{B^0} \quad \Rightarrow B=1-\frac{erfc\left(\frac{1-\eta}{2\sqrt{\tau_s}}\right)}{erfc\sqrt{\bar{\alpha}}} \qquad 0\le\eta\le\frac{\lambda_s}{R} \tag{42}$$

The last two sets of substitutions can be done together to give the final result:

$$\left.\begin{array}{l}\textit{Substitute}\\ u=A\eta\\ z=1-\eta\end{array}\right\} \Rightarrow u=(1-z)\left[1-\frac{erf\left(\frac{z}{2\sqrt{\tau_s D_1/D_2}}\right)}{erf\sqrt{\frac{\bar{\alpha}}{D_1/D_2}}}\right] \qquad 0\le z\le 1-\frac{\lambda_s}{R} \tag{43}$$

$$\theta = B\eta \quad \rightarrow \theta = (1-z)\left[1 - \frac{erfc\left(\frac{z}{2\sqrt{\tau_s}}\right)}{erfc\sqrt{\alpha}}\right] \qquad 1 - \frac{\lambda_s}{R} \le z \le 1 \tag{44}$$

4.3 Overall H_2S Mass Balance

In the previous chapter, the algorithm for calculating the amount of H_2S absorbed by a single droplet was presented in equations 11 and 12. Here these results will be used to generate an equation for the surface concentration of the H_2S in the liquid over time. At every time step in the calculations, equation 12 is employed for each of the droplet sizes to calculate the amount of H_2S each droplet has absorbed, and then the results are extended over the entire spray to give the total amount of H_2S absorbed. This value is then subtracted from the original amount of H_2S in the gas to give the amount remaining, which then can be used to give the desired new value of the H_2S surface concentration in the liquid.

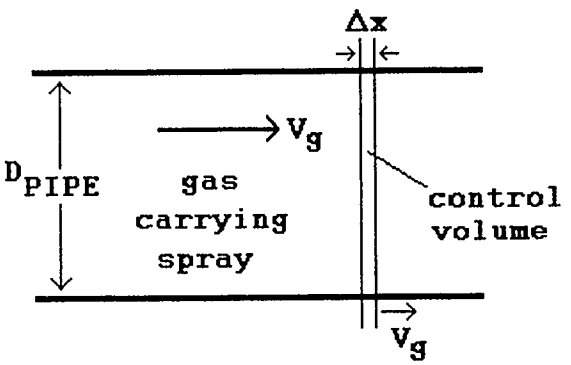

Figure 7: Schematic of Pipe

Figure 7 shows a schematic of the section of the two

phase mixture over which the mass balance is being performed. The width Δx is assumed small enough that conditions within the control volume are uniform. In its raw form, the overall H_2S balance equation is then:

$$\left[\frac{a}{A^*}\Big|_0\right]A^*K_{EQM}\Delta x\frac{\pi}{4}D_{PIPE}^2(1-V_{FL}) =$$
$$A^*K_{EQM}\Delta x\frac{\pi}{4}D_{PIPE}^2(1-V_{FL}) -$$
$$\sum_{K=1}^{N_{DROP}}\left\{\left[\int_{\lambda(t)}^{R}a(r)4\pi r^2dr + B^0\frac{4}{3}\pi R^3 - \int_{0}^{\lambda(t)}b(r)4\pi r^2dr\right]_K\right. \qquad (45)$$
$$\left.*\frac{V_{FL}\Delta x\frac{\pi}{4}D_{PIPE}^2\{V[(D_{LIM})_K] - V[(D_{LIM})_{K-1}]\}}{\frac{4}{3}\pi R_K^3}\right\}$$

Here K_{EQM} is a dimensionless conversion factor between equilibrium gas and liquid phase H_2S concentrations, and V_{FL} is the volume fraction of the liquid in the two phase mixture. The first part of the summation term is exactly equation 12. This part gives the amount of H_2S each droplet has absorbed, and the second part multiplies this by the total number of droplets for each size. This second quantity is found as the total liquid volume in the control volume times the fraction of the volume of the spray represented by the current drop size, divided by the volume of each droplet. The values of $V[(D_{LIM})_K]$ and $V[(D_{LIM})_{K-1}]$ are found from the Rosin-Rammler cumulative volume distribution (equation 6) using diameters found from the cumulative surface area distribution (equation 10).

In order for the equation to be of direct use, the

concentrations in the summation term of equation 45 must be converted to their dimensionless equivalents which are actually calculated. Doing this results in an alternate form of equation 12:

$$(H_2S \text{ absorbed}) = \frac{4}{3}\pi R^3 A^* \frac{B^0}{A^*}\left[1+\frac{3}{B^0/A^*}\int_0^{\bar{\lambda}(\tau)} u(z)\,(1-z)\,dz - 3\int_{\bar{\lambda}(\tau)}^{1} \theta(z)\,(1-z)\,dz\right] \quad (46)$$

Substituting this back into equation 45 and simplifying:

$$u|_{z=0} = 1-\frac{B^0/A^*}{K_{EQM}}\frac{V_{FL}}{1-V_{FL}} * \sum_{K=1}^{N_{DROP}}\left[1+\frac{3}{B^0/A^*}\int_0^{\bar{\lambda}(\tau)} u(z)\,(1-z)\,dz - 3\int_{\bar{\lambda}(\tau)}^{1} \theta(z)\,(1-z)\,dz\right]_K * \{V[(D_{LIM})_K] - V[(D_{LIM})_{K-1}]\} \quad (47)$$

The term which the sum is multiplied by can be simplified to remove the quantities of K_{EQM} and V_{FL}. It was mentioned in the previous chapter that one of the parameters which characterizes the system is the ratio of the total molar feed flowrate of MEA to that of H_2S in the two phase mixture (a quantity hereafter referred to as M_{RATIO}). This quantity is simply the ratio of the bulk concentration of MEA in the liquid times the total liquid volume in the control volume divided by the bulk H_2S concentration in the gas phase times the total gas volume:

$$M_{RATIO} = \frac{B^0 V_{FL} \Delta x \frac{\pi}{4} D_{PIPE}^2}{A_{BULK} \Delta x \frac{\pi}{4} D_{PIPE}^2 (1-V_{FL})} \quad (48)$$

By definition, A^* is the liquid phase concentration that would be in equilibrium with the concentration of H_2S in the feed

gas, and so $A_{BULK} = A^* K_{EQM}$. Putting this into equation 48 gives:

$$M_{RATIO} = \frac{B^0/A^*}{K_{EQM}} \frac{V_{FL}}{1-V_{FL}} \tag{49}$$

This expression appears explicitly in equation 47. As a result of this, the final form of equation 47, the overall H_2S mass balance equation, is:

$$u|_{z=0} = 1 - M_{RATIO}$$

$$* \sum_{K=1}^{N_{DROP}} \left[1 + \frac{3}{B^0/A^*} \int_0^{\bar{\lambda}(\tau)} u(z)\,(1-z)\,dz - 3 \int_{\bar{\lambda}(\tau)}^{1} \theta(z)\,(1-z)\,dz \right]_K \tag{50}$$

$$* \{ V[(D_{LIM})_K] - V[(D_{LIM})_{K-1}] \}$$

CHAPTER 5

COMPUTER PROGRAM

5.1 Introduction

A Fortran computer program was written on the University of Calgary AIX system to perform the calculations involved in solving the system model. The high level structure of the program, with all major program blocks included, is outlined in Figure 8.

The procedure is that following the user inputs, the specified spray is discretized into a small number of representative droplet sizes, and then initial profiles are calculated for all the droplets. An overall H_2S mass balance is performed using the initial profiles to find the surface concentration for the start of numerical calculations. A test is performed on the results of this step to ensure the surface concentration of H_2S at the end of the analytical calculations is not below 0.96. If it is, the program stops. This is done to try to assure the accuracy of the initial profiles, which are calculated with the assumption that the surface concentration of H_2S is fixed. Next various initializations are performed, including setting the time to that of the end of the analytical calculations.

The time loop is then entered. Inside this loop is an inner loop, within which the concentration profiles and reaction front positions for each droplet size are calculated

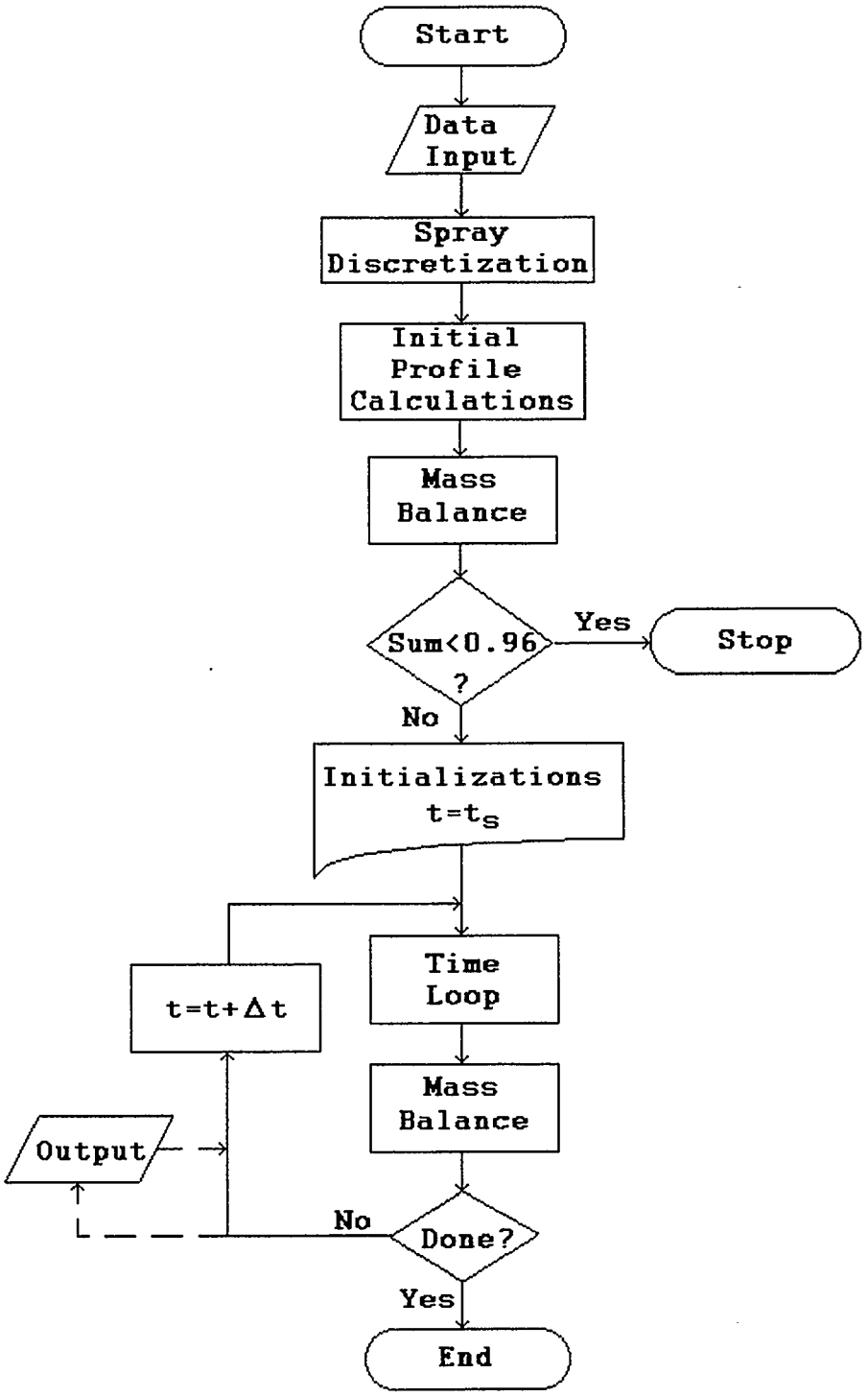

Figure 8: Major Program Blocks

for the unknown time level. The newly calculated profiles are then fed into the H_2S mass balance routine to recalculate the outside H_2S concentration. A test is performed to check if the desired stopping position has been reached, and if not a new time step is begun. If the end has been reached, the procedure stops. Output is periodically performed. The major sections of the program are described below in detail.

5.2 Inputs

The user inputs consist of ten quantities:

1. The ratio of the liquid phase diffusivity of H_2S to that of MEA (D_1/D_2).
2. The dimensional MEA diffusivity, in units of m^2/s (D_2).
3. The ratio of the maximum liquid phase concentration of MEA to that of H_2S (B^0/A^*).
4. The Rosin-Rammler size parameter X, in units of 10^{-6} m.
5. The Rosin-Rammler distribution parameter N.
6. The number of droplet sizes the spray is to be discretized into (N_{DROP}).
7. The number of subintervals to divide the radius of the smallest droplet into $(N_{IVAL})_1$.
8. The molar feed ratio of MEA to H_2S (M_{RATIO}).
9. The gas velocity, in units of m/s (V_g).
10. The downstream distance to stop calculations at, in m.

The inputs are essentially of two types, those which characterize the system (#1 - #5, #8, #9) and those which

define the calculation to be performed (#6, #7, #10). In keeping with the pattern of using dimensionless variables wherever possible, three of the inputs are dimensionless ratios. For input #6, the more droplets the user specifies the spray be discretized into, the closer the spray is represented, but the longer calculation times will be. To reduce calculation times for a certain value of N_{DROP}, the value of input #7 should be made as small as possible. The lower limit is based on the new surface concentration calculated from the initial profiles - if the number of intervals is too small, this number will fall below the limit of 0.96. Finally, in a real scrubber input #10 would correspond to the distance between the start of the region of complete mixing in the scrubber and where the atomized scrubbing solution is removed from the gas stream.

5.3 Spray Discretization

Figure 9 shows the expanded flowchart for the spray discretization block of the process. The procedure consists of two sections, the subdivision of the surface area distribution into equal fractions, and then the determination of the Sauter mean diameters of each of the subdivisions. In the first section, a number of droplet diameters equal to the number of droplets the spray is to be discretized into are found. The diameters are calculated so that between adjacent pairs an equal fraction of the total surface area of the spray lies.

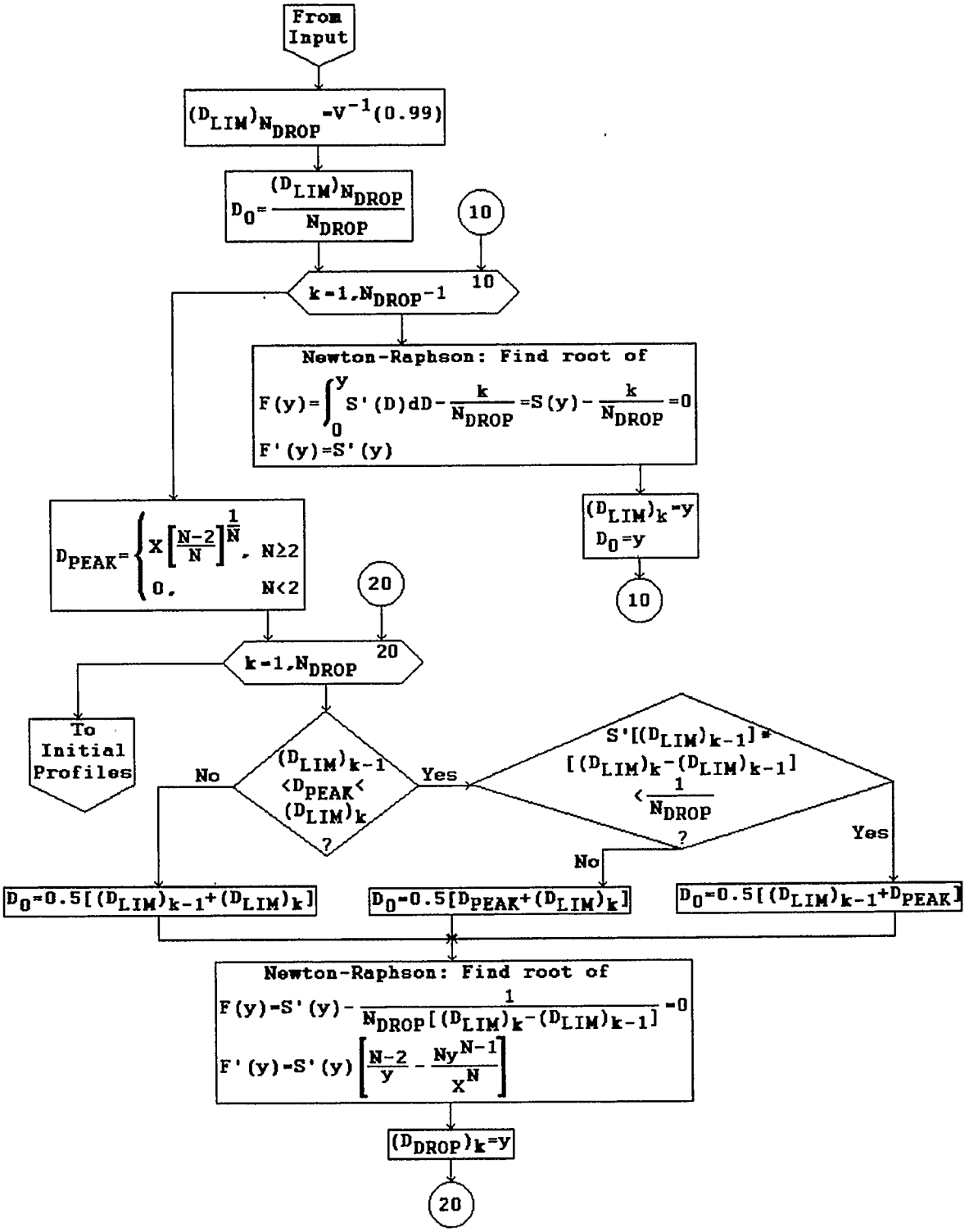

Figure 9: Spray Discretization Block

The low diameter is of course 0, and the high diameter is calculated as that below which 99% of the volume of the spray falls, from equation 6. In practice this diameter gives about 99.75% of the surface area of the spray. The limiting diameters are calculated by a Newton-Raphson algorithm, solving an expression using the surface area distribution of equation 10. The initial guess for the first diameter is simply taken as the high diameter divided by the number of droplets, and for later diameters the result for each diameter is taken as the initial guess for the calculation of the next.

In the second part of the routine, the diameters that will actually be used in the mass transfer calculations are determined. The mean value theorem for definite integrals is employed here. This theorem states that in an interval between any two points of a continuous function there is a third point whose functional value times the width of the interval is equal to the area beneath the curve between the first two points. Here the first two points are consecutive diameters calculated in the first section of the block, and the third is the desired droplet diameter. In this way the calculated droplet diameters are actually Sauter mean diameters of the subdivisions of the spray they are found from.

The diameters are found by a Newton-Raphson root finding procedure. Normally initial guesses are simply the midpoints of the interval. However, when the Rosin-Rammler distribution parameter N is greater than 2, there is a peak in the surface

area distribution function. In the interval containing the peak, there can potentially be two diameters which satisfy the mean value theorem. The test for whether or not there will be two diameters is if the lesser boundary diameter times the interval width is less than the area beneath the curve in the interval; if yes there are two potential answers, if no only one. If the result of this test is no, the diameter will lie between the peak diameter and the larger boundary diameter, so the midpoint of this interval is taken as the initial guess. If the result is yes, the smaller diameter is chosen as it gives faster mass transfer. In this case the midpoint of the interval between the lower boundary diameter and the peak is used as the initial guess.

5.4 Initial Profiles

Figure 10 shows the complete flowchart for the initial profile calculation block of the program. In this block, necessary initial calculations are first performed, and then the concentration profiles are computed for all the droplet sizes using the converted analytical solutions for instantaneous reaction in a semi-infinite rectangular environment. The first calculation is a Newton-Raphson root solution for the parameter α, the dimensionless reaction front speed factor. The equation solved is equation 40. The result of this is then used to find the absolute and dimensionless times for the analytical calculations. For the smallest

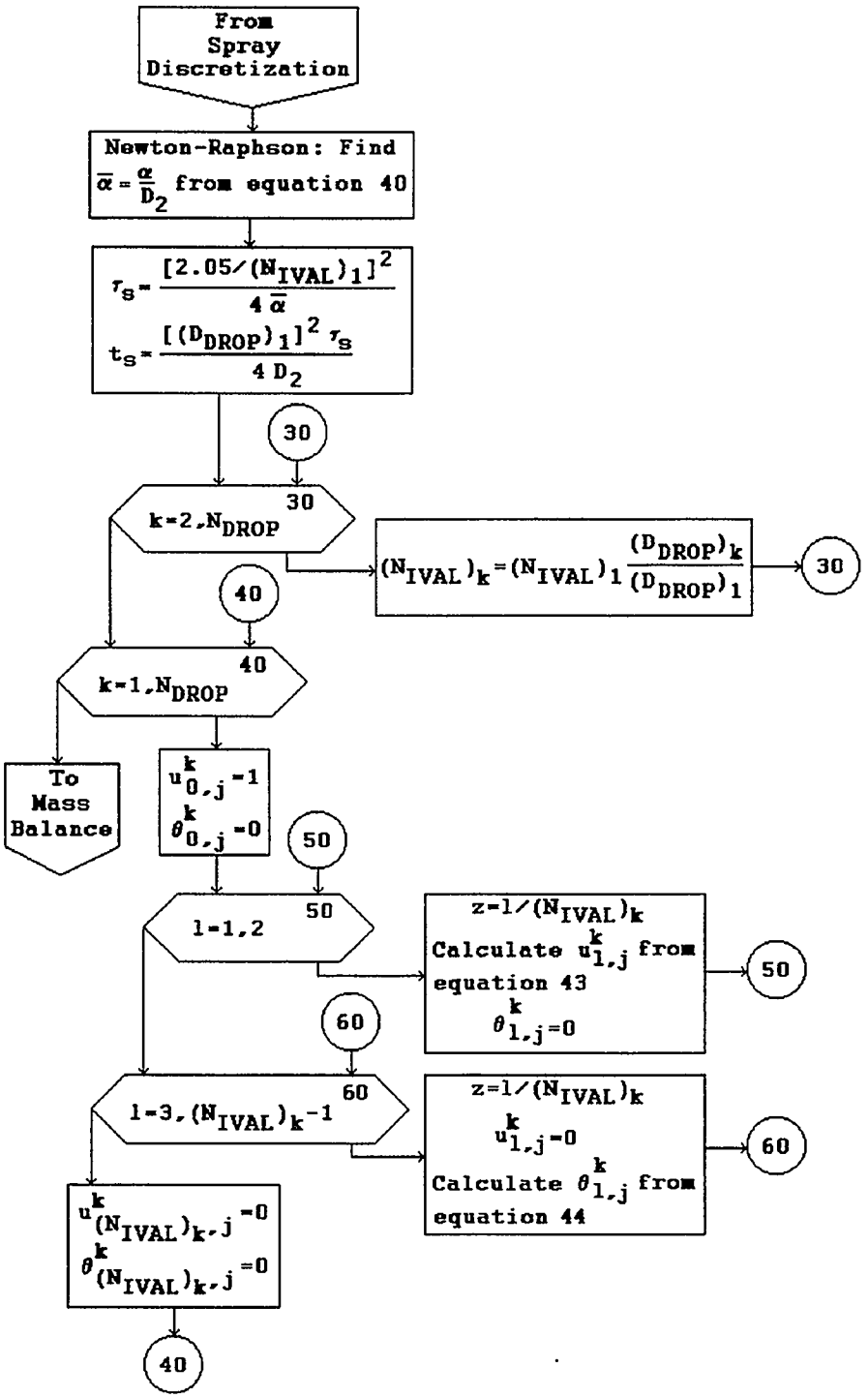

Figure 10: Initial Profile Calculation Block

droplet, the depth of the reaction front for which the analytical calculation is performed is 2.05 space intervals. This number is chosen as the minimum value which will give a u profile of four points, which from practice always gives stable starting results from the numerical routine. The dimensionless time for the smallest droplet is calculated from this and the number of space intervals specified by the user. For the same reason of stability, the number of space intervals deep the reaction fronts are for the larger droplets is also specified as 2.05, and the number of space intervals for each is computed to correspond. The equation used here is determined by setting the formula for the absolute starting time for a droplet equal to that for the first droplet, and solving for the unknown of the number of space intervals for the larger droplet. The consequence of this is that the absolute space grid widths for all the droplets (in m) are equal.

Next the profiles themselves are actually found. The surface concentration of H_2S is set at 1, its initial value. For all the droplets, the profiles are found using equations 43 and 44, with concentrations in regions where the respective components do not exist set equal to zero. For droplets other than the smallest, the dimensionless times used are converted from that for the smallest droplet as follows:

$$(\tau_s)_k = (\tau_s)_1 \left(\frac{(D_{DROP})_1}{(D_{DROP})_k} \right)^2 \qquad (51)$$

All the dimensionless times of course correspond to the same absolute time. In the last step, the values of θ at the centre of the droplets are all set to 0, corresponding to the boundary condition there.

5.5 Mass Balance

Figure 11 shows the flowchart of the mass balance routine used in the calculations. In this procedure the new value of

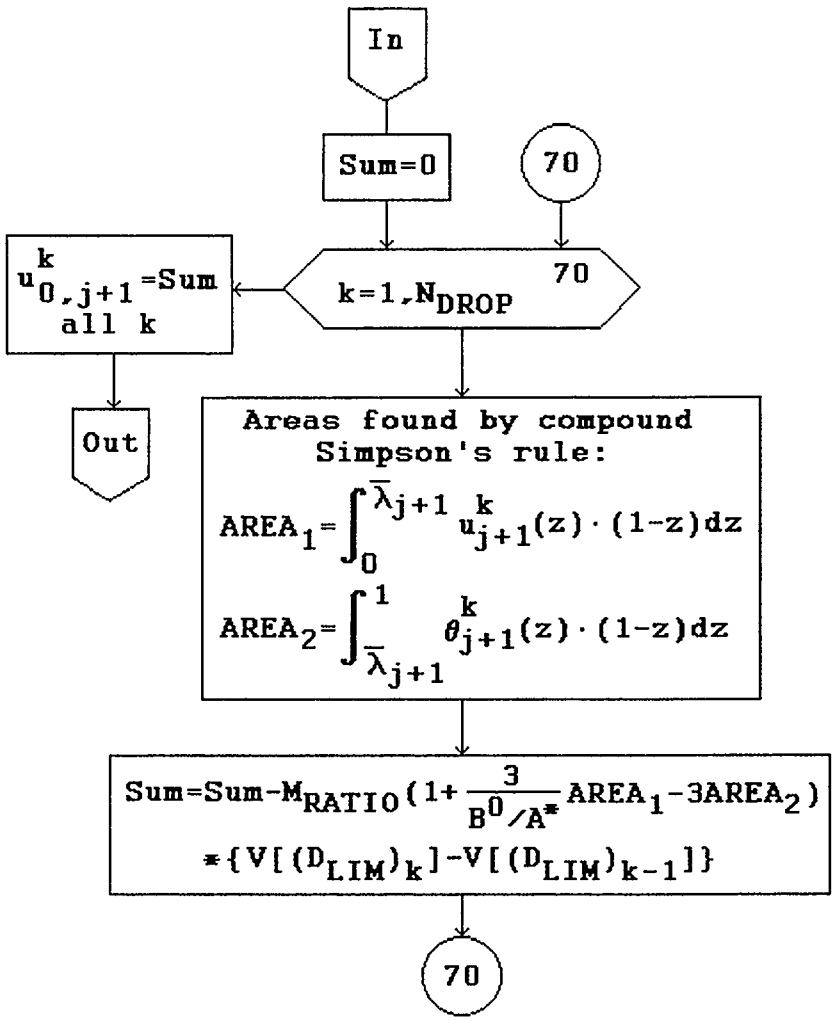

Figure 11: H_2S Mass Balance Block

the surface concentration of H_2S is calculated by the series

given in equation 50. For each droplet size the areas in equation 50 are found numerically by the compound Simpson's rule. Once the series is complete, the new concentration value is entered into all the droplet concentration profiles.

5.6 Time Loop

Figure 12 shows the flowchart of the heart of the program, the time loop where in each time step the complete concentration profiles for all the droplets are calculated along with updated reaction front positions. With these new numbers an H_2S mass balance is performed and a new value of the surface concentration calculated before the next time step is begun.

The two stages of the loop are carried out for each droplet size in an inner loop. The values of u and θ for each space grid line are calculated for the new time step in loops over their respective ranges of application using equations 23 and 27 respectively. The values of the profiles at the grid lines surrounding the reaction front are calculated from equations 32 and 33. The values of $(\Delta\tau)_k$ used in these equations are calculated as part of the initializations to represent the same absolute time step size. The value of $(\Delta\tau)_1$ is specified as half the lesser of the values from equations 25 and 29. Values for the other droplets are then found from this by the method of equation 51, the square of the ratio of diameters.

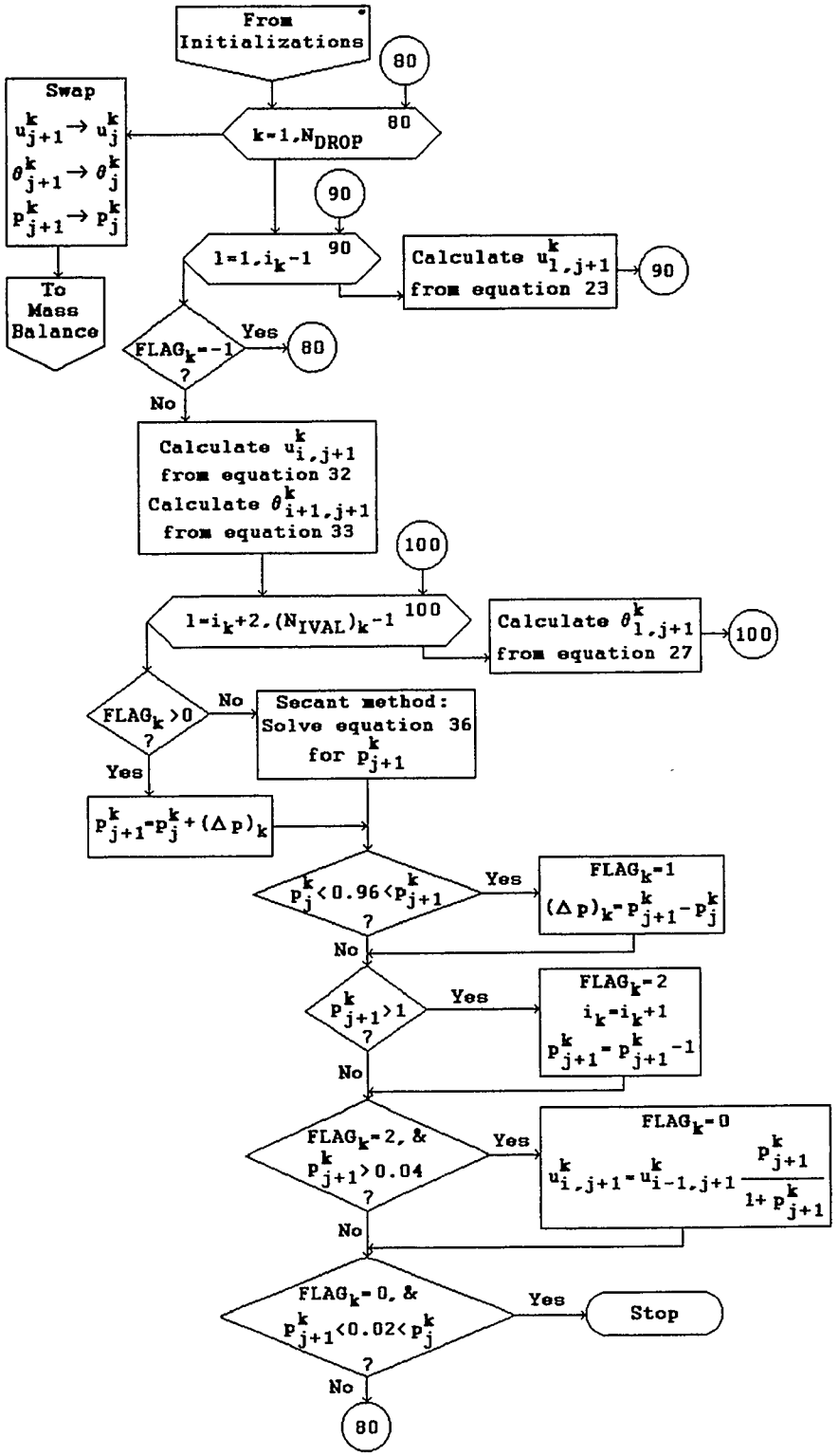

Figure 12: Time Loop Block

In the reaction front calculation routine, a quantity called $FLAG_k$ is used to keep track of the current state of calculations for each droplet. This quantity can take on four values: 0, 1, 2, and -1. A value of zero indicates things are normal, and the reaction front position is found from equation 36 by the secant method, using the two previous front positions for the current drop as initial guesses. When the value is -1, more than 99.95% of the MEA originally present in the droplet has been consumed, and so calculations are halted. The H_2S profile continues to be calculated though, but the reaction front position is left at its final value.

Values of 1 or 2 for the flag variable indicate that the marching method is being used to calculate the reaction front position, 1 meaning that p_{j+1} is between 0.96 and 1, and 2 meaning that it is between 0 and 0.04. The marching method is initiated when a calculated value of p_{j+1} becomes greater than 0.96. From this point on, the reaction front position for that droplet is incremented in following time steps by the amount it went up in the step it crossed 0.96. Due to the unstable results they give, during the marching procedure equation 33 is not used to calculate $\theta_{i+1,j+1}$ when $FLAG_k$ is 1, and equation 32 is not used for $u_{i,j+1}$ when $FLAG_k$ is 2. The values are simply set to zero. When p_{j+1} is incremented across unity, its value is reduced by one, the reaction front grid line index i_k is incremented, and $FLAG_k$ is changed from 1 to 2. When the value becomes greater than 0.04, the marching method is ended

by the value of $FLAG_k$ being changed back to 0. A new value of $u_{i,j+1}$ is also specified at this point, using linear interpolation. At the end of the time loop, the process symbolically moves ahead one time step by the calculated numbers for the time level j+1 being copied into the corresponding variables for time level j.

One final test is performed at the end of the loop to stop calculations if the reaction front of a droplet is moving backwards towards a grid line. When this is happening, the calculations will crash unless stopped.

CHAPTER 6

RESULTS AND DISCUSSION

6.1 Introduction

In this chapter results from the Fortran program are presented. The output are discussed in the order they are generated by the program. Droplet discretization results are presented for four different runs, and then concentration profiles for one run are given for two of the droplets. Plots of the reaction front positions for three runs are presented, and a discussion of the questions raised follows. For six runs the final output of the program, the surface concentration of H_2S versus distance, are given. Finally, discussion of other relevant issues is made, including the calculation times and errors.

6.2 Spray Discretization

Four calculated sets of droplets are presented in Figures 13 - 16. The figures show 4 and 8 droplets calculated from two different sets of Rosin-Rammler parameters, the first being X = 76 μm and N = 2.14 and the second X = 80.45 μm and N = 2.01. All four graphs show that the droplets are clustered around the peaks of the curves, which is expected since the majority of the area is there. The shape of the Rosin-Rammler surface area distribution equation curves are illustrated in these figures. It can be seen that the curves rise sharply from zero

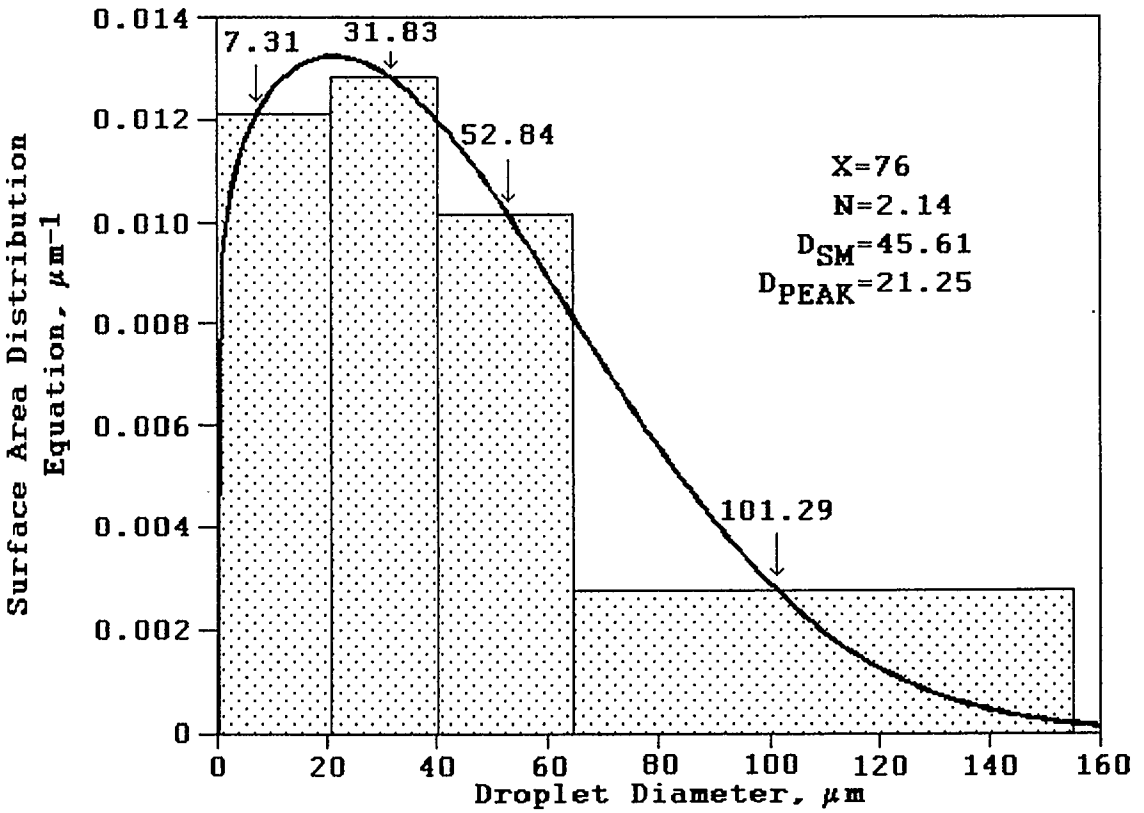

Figure 13: Droplet Profile for 4 Drops, X = 76 μm, N = 2.14

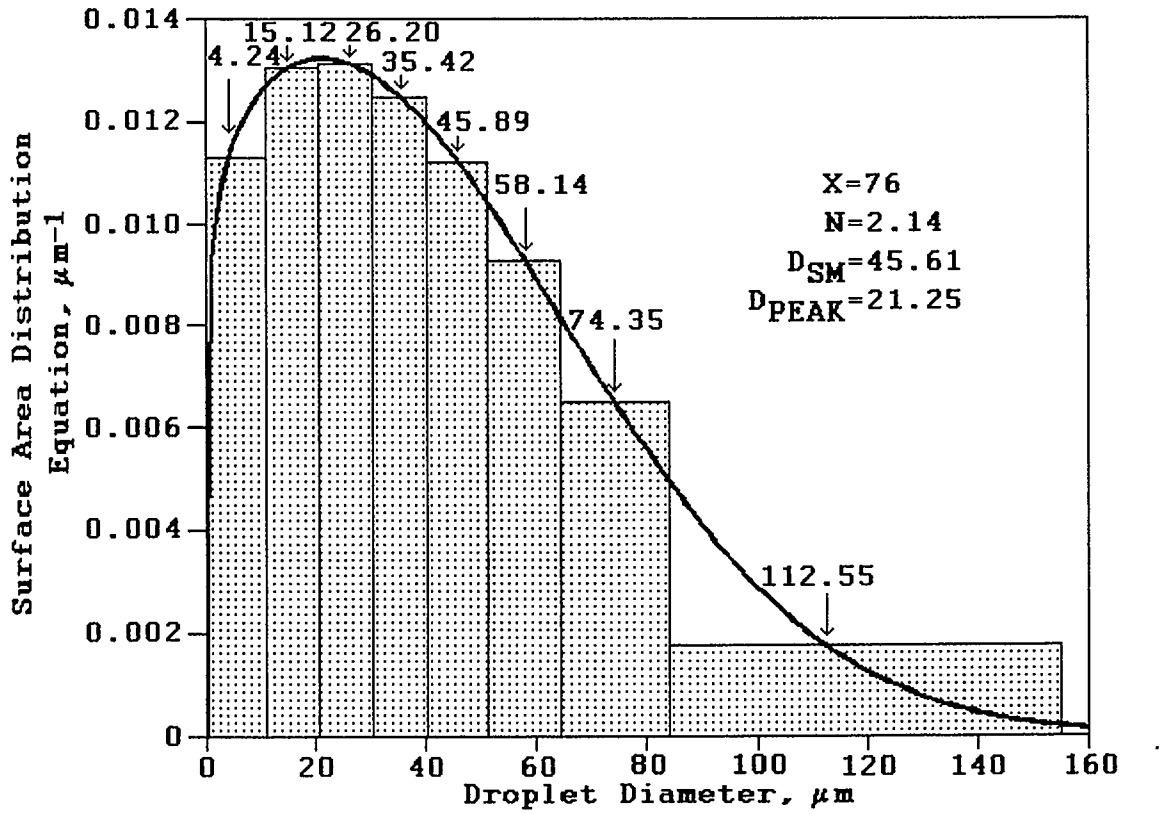

Figure 14: Droplet Profile for 8 drops, X = 76 μm, N = 2.14

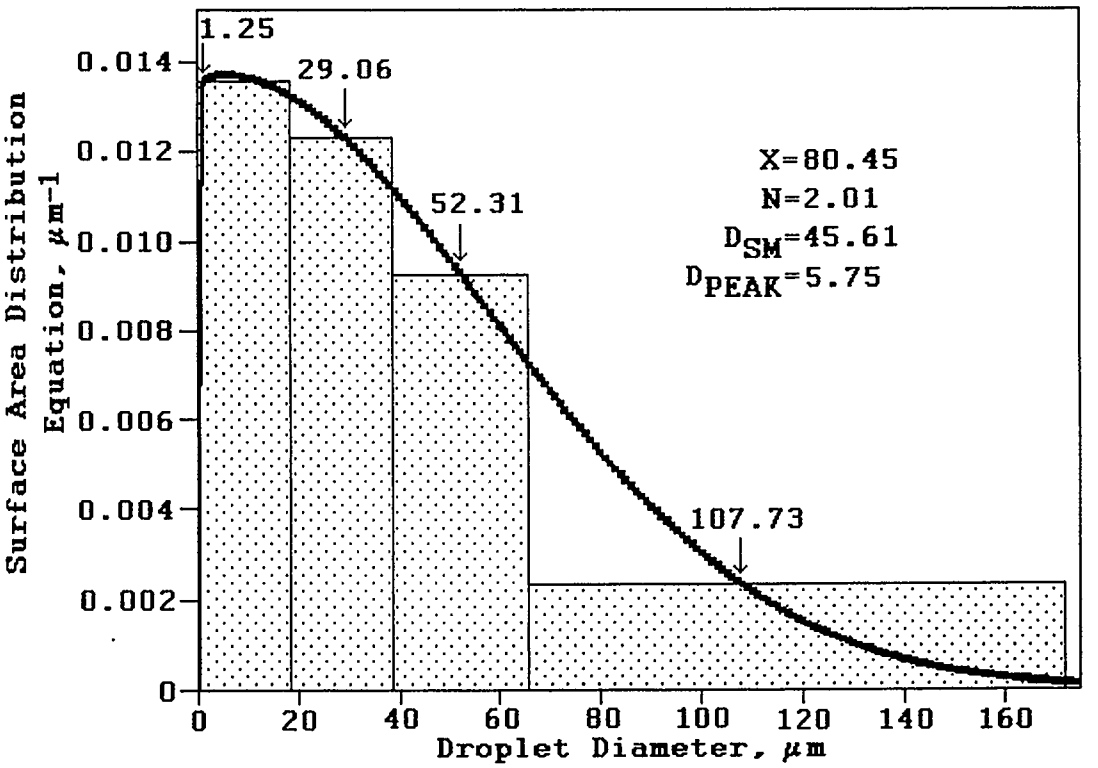

Figure 15: Droplet Profile for 4 drops, X = 80.45 μm, N = 2.01

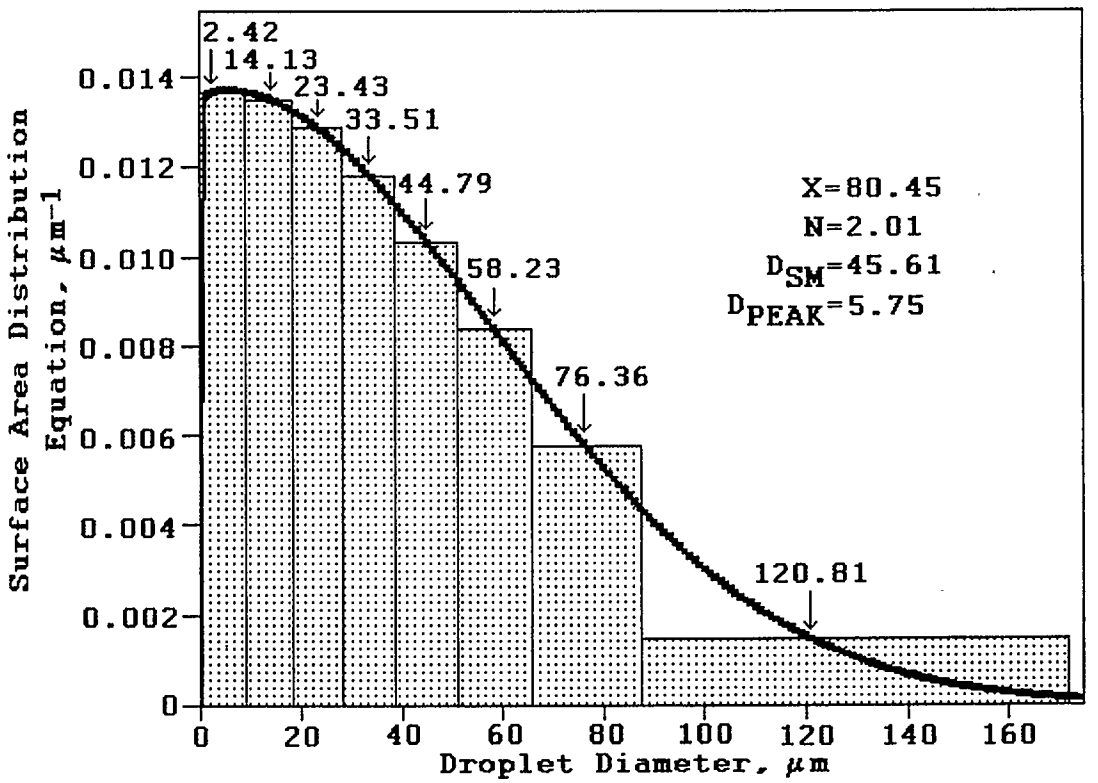

Figure 16: Droplet Profile for 8 drops, X = 80.45 µm, N = 2.01

to a peak, then taper off to zero as the diameter increases. Comparing the two curves shows how as N approaches 2, the peak approaches zero. For values of N less than 2, the peak is at zero. The actual droplet diameters used in the calculations are indicated in the diagrams. The shaded bars illustrate how each diameter represents the area beneath the curve over its respective interval of diameters. Of special note is the bar for the smallest diameter in Figure 15. As can be seen it crosses the curve at two points, indicating two diameters exist which would give the correct area beneath the curve. As mentioned before, the smaller diameter is chosen for faster mass transfer.

The width of each bar in the diagrams is the distance between boundary diameters calculated by solving the cumulative surface area distribution of equation 10 for the appropriate fraction of the total surface area of the spray. Figure 17 shows a plot of this equation for X = 76 μm and N = 2.14. The figure shows how for a system of 4 droplets the total surface area is divided into quarters. The uppermost diameter as mentioned before is calculated as that which gives 99% of the total volume of the spray from equation 6. In this case this diameter gives 99.73% of the total surface area.

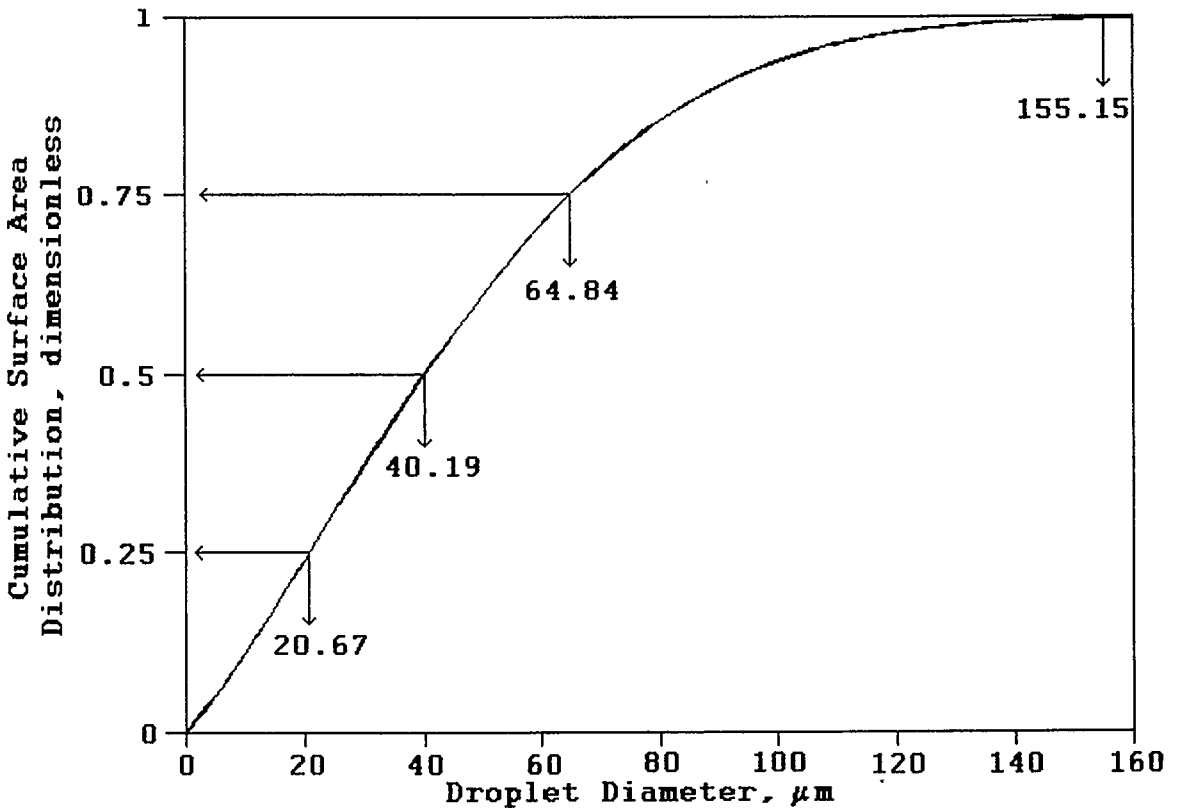

Figure 17: Cumulative Surface Area Distribution for X = 76 μm, N = 2.14

6.3 Time Loop Results

6.3.1 Runs

A series of six runs was performed using the Fortran program. The inputs for the runs are chosen as typical values for commercial scale H_2S scrubbing by an MEA spray, and are shown in Table 1. The common inputs for all six are the MEA

Table 1: Inputs for Runs

Input Quantity	Value(s)
MEA diffusivity (D_2)	$7.68*10^{-10}$ m^2/s
Diffusivity ratio (D_1/D_2)	2.3
Concentration ratio (B^0/A^*)	7.5
Rosin-Rammler parameters (X, N)	(76 μm, 2.14), (80.45 μm, 2.01)
Molar feed ratio (M_{RATIO})	2.5, 0.75
Gas velocity (V_g)	13.716 m/s

diffusivity, the liquid phase diffusivity ratio, the ratio of initial liquid phase concentrations, and the gas velocity. The MEA diffusivity is specified as $7.68*10^{-10}$ m^2/s, which is an estimate calculated from the correlation of Wilke and Chang (Treybal, 1987, pg. 35). In the calculation, the solvent is taken as water, the temperature 298 K, and an estimate of the solution viscosity of $1.5*10^{-3}$ kg/(m·s) (Kohl and Riesenfeld, 1979, pg. 56) is used along with an estimate of the density of pure MEA at its normal boiling point of 950 kg/m^3 (Younger, 1977, pg. 16-8). The diffusivity ratio is calculated from this number and a value of the diffusivity of H_2S in water of $1.77*10^{-9}$ m^2/s (Weast and Astle, 1982, pg. F-50), giving a

result of 2.3. The ratio of initial liquid phase concentrations is based on a 15 wt% solution of MEA (Kohl and Riesenfeld, 1979, pg. 38), and a gas stream at 298 K and 6.307 MPa (900 psig), with 5 mole % H_2S. The solubility of H_2S is taken from Wankat (1988, pg. 474). The resulting value used is 7.5. Finally, the gas velocity used is 13.716 m/s (45 ft/s), which is the same as that in one of the Waterloo scrubber units in commercial use (Spink, D.R., 1992).

Four of the runs are performed for a value of 2.5 for the molar feed ratio of MEA to H_2S (M_{RATIO}). This value is the same as that typically used in MEA tray scrubbers (Younger, 1977, pg. 16-9). The other two are run at M_{RATIO} = 0.75. This value is used for two reasons. The first is that in practice a large MEA - H_2S ratio may be difficult to achieve considering the amount of material that would have to be sprayed. The second reason is to illustrate how differently the calculations proceed according to which side of 1 M_{RATIO} lies.

The six runs are all performed for either one or the other of the two sets of Rosin-Rammler parameters for which the spray discretization results are presented in the previous section. The first set of parameters, X = 76 μm and N = 2.14, are numbers actually measured from one of the nozzle types used in Waterloo scrubbers (Brena de la Rosa, 1987). The numbers give a Sauter mean diameter for the spray of 45.61 μm, which is in the range recommended by Turbotak, the company marketing the Waterloo scrubber (Spink, D.R., 1992). The

second pair of parameters is X = 80.45 μm and N = 2.01. These give the same Sauter mean diameter of 45.61 μm as for the previous set, but a considerably different spray profile.

6.3.2 Concentration Profiles

A graph of three concentration profiles from the smallest droplet and one from the largest droplet for the run with X = 76 μm and N = 2.14 is shown in Figure 18. The concentrations of both MEA and H_2S are plotted as fractions of their maximum values. Where the curves touch the dimensionless radius axis is the position of the reaction front. To the left of this is the MEA profile and to the right the H_2S profile. For all the curves no value of the concentration exists for a dimensionless radius of exactly zero. This is due to the substitutions made to change the variables for MEA concentration and distance - at $\eta = 0$, $\theta^k = 0$, which when converting back to actual concentration gives 0 over 0.

The three curves for the small droplet correspond to the start of the calculations, the end (for that droplet), and somewhere in the middle. The first curve is that given by the initial profile routine. As can be seen, the deflection of the MEA curve from the initial condition does not extend very far into the droplet. This indicates that the assumption that for short times the droplets can be viewed as infinitely deep slabs is a safe one to make. The second curve is for 50% consumption of the MEA in the droplet. At this point the MEA

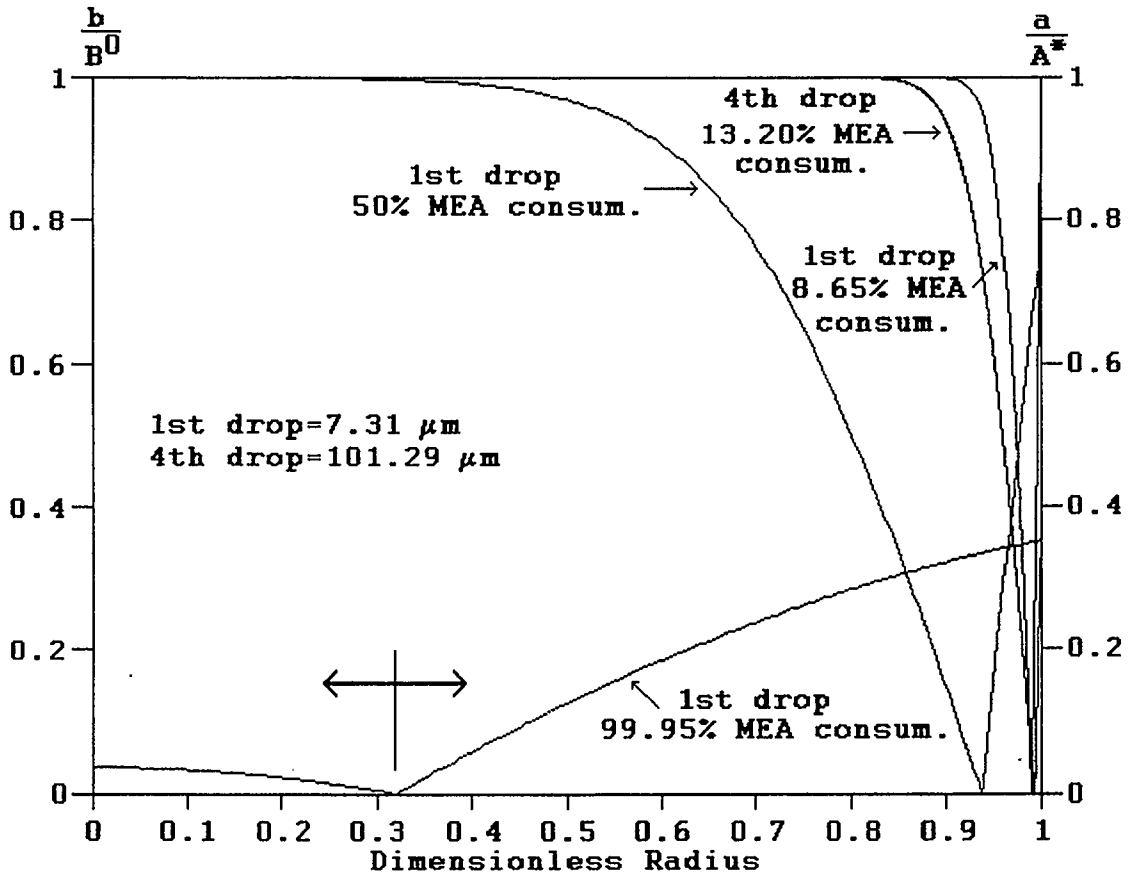

Figure 18: Concentration Profiles

concentration at the centre of the droplet is still at its initial value. The final curve is for 99.95% MEA consumption. As can be seen the reaction front has penetrated nearly to the centre of the droplet, and the MEA profile has practically disappeared. The curve for the large droplet is for the same absolute time as this curve, and it shows how great the difference is between how the mass transfer processes progress in the two droplets.

In all the curves the MEA profiles are convex, corresponding to depletion, which is what occurs due to consumption by chemical reaction. Also in the curves, the H_2S gradient at the reaction front is greater than that for MEA, which makes sense since in equation 15 D_1/D_2 is less than B^0/A^*. Except for the last curve, all the H_2S profiles are essentially linear, indicating that the mass transfer is almost at steady state. This can be attributed to the fact that the H_2S diffusivity is much larger than that of MEA. In the third curve for the small droplet, the H_2S profile is convex, indicating depletion. Because the reaction has ceased in the droplet, the H_2S that in diffusing towards the centre would formerly have replaced the amount consumed now goes towards raising the concentration there. At long times the profile will become flat as the droplets approach saturation.

6.3.3 Reaction Front Positions

6.3.3.1 Numerical Issues

The calculation of the position of the reaction front for droplets is the only iterative procedure in the time loop. All the other calculations are carried out in simple loops. The secant method procedure used to solve equation 36 for the updated reaction front position is quite well behaved, converging in 3 or 4 iterations each time.

The marching method used to increment reaction front positions across space grid lines is necessary as mentioned before due to the asymptotes of equation 36 at $p_{j+1} = 0$ and 1. By this method reaction front positions within 0.04 grid widths of any grid line are found. Following the end of the use of the marching method to calculate reaction front positions, results from the secant method calculation briefly oscillate. The oscillations are stable, and after a short time the calculated value of the reaction front position returns to the path it had been taking before. The reason for this phenomenon is the uncertainty in the value of $u_{i,j+1}$ in equation 36, for which the value is computed by linear interpolation at the end of the marching method procedure. The amplitude of the oscillations are smaller for smaller time step sizes, and in the runs described here the time steps are so small that the oscillations are essentially negligible.

There are two instances in the reaction front position calculations when extraordinary measures are taken to prevent

errors. The first is when the MEA in a droplet is approaching complete consumption. As the reaction front approaches the centre of a droplet, due to the diminishing radius less and less MEA is required to be consumed for the front to move forward an amount. Thus the front begins to accelerate. To prevent problems that might arise from the reaction front moving too quickly, calculation of front positions for droplets are halted once the percent consumption of MEA exceeds 99.95%. To allow later effects to be caught, the H_2S profiles are continued to be calculated for these droplets though.

The second special case is exclusive to when M_{RATIO} is greater than unity. Under this circumstance the limiting reagent in the process is H_2S. If the mass transfer process are allowed to continue indefinitely, eventually all the H_2S will be absorbed from the gas into the liquid phase and consumed in reaction with MEA. What will be left in the droplets are flat profiles of the excess MEA, with the leftover concentrations being highest in the largest droplets and decreasing by droplet diameter to zero for the small droplets in which the MEA has been completely consumed. In the mass transfer process reaction fronts in the droplets are initially moving forward, but at the finish they have disappeared completely. At some intermediate point then they must have turned around and begun to move the other direction.

The way this reversal works is that based on the amount

of MEA remaining in a drop, at some point the surface concentration will have dropped so low that the H_2S concentration gradient at the reaction front will only be able to remain equivalent to the MEA gradient if the front goes backwards. This happens sooner for the larger droplets as they will contain more MEA than the smaller droplets at the same absolute time, and hence for the same value of the surface concentration the MEA gradients will be larger. As the outside H_2S concentration continues to fall, eventually this occurs for all unconsumed droplets. The problem this creates is that at some point the position of one of the reaction fronts in the droplets will have decreased until it is approaching a grid line. Because of the asymptote in equation 36 at $p_{j+1} = 0$, it will never be able to cross. At this point the calculations have to be halted to prevent unpredictable results. A potential solution to this problem does exist - the marching method could be extended to work for reaction fronts crossing grid lines in the other direction. In the program this would require a mirroring of all the marching method blocks in Figure 12 but for motion in the opposite direction.

6.3.3.2 Calculated Results

Figures 19 and 20 show the positions of the reaction fronts of the droplets for the two runs at X = 76 μm, N = 2.14, and M_{RATIO} = 2.5 for 4 and 8 droplets respectively. In the figures the curves fall vertically in order of droplet

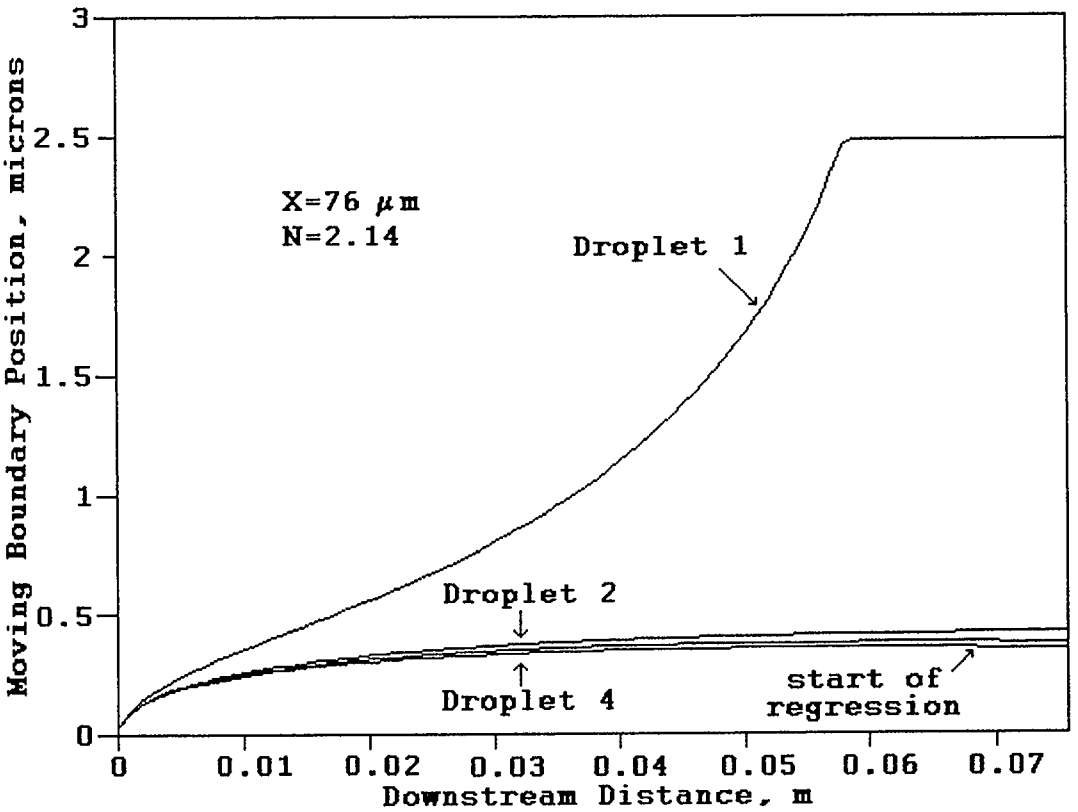

Figure 19: Reaction Front Positions for 4 Droplets at M_{RATIO} = 2.5

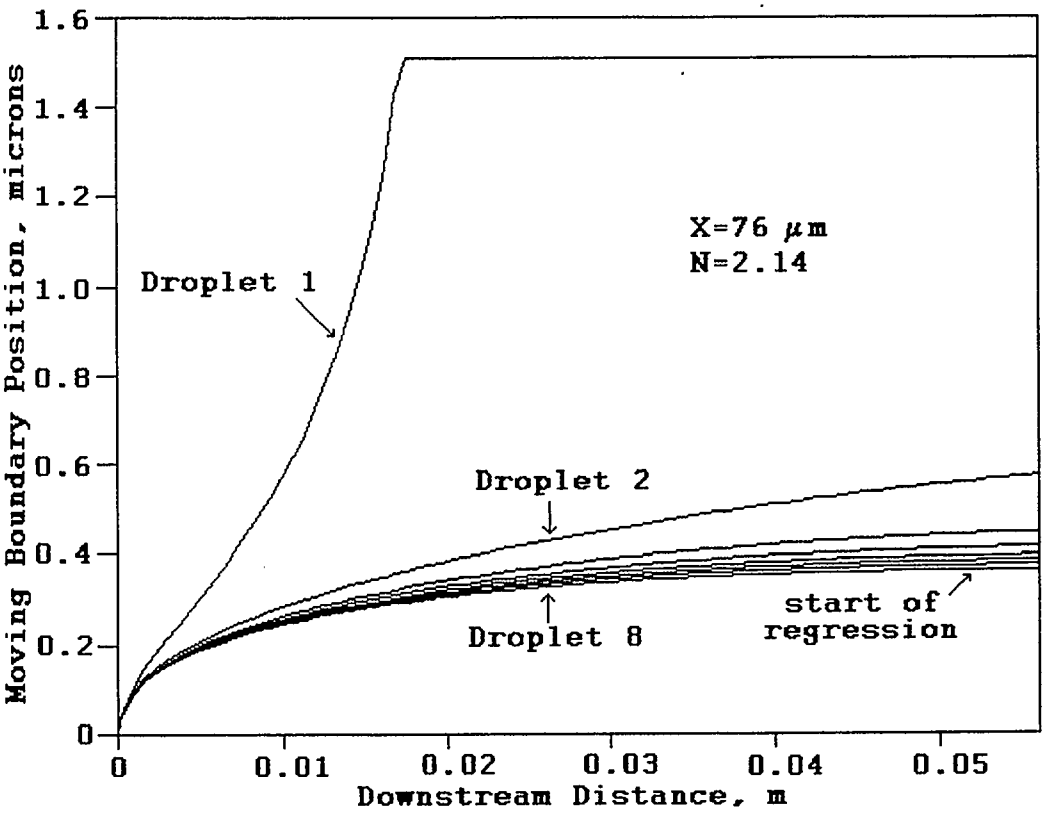

Figure 20: Reaction Front Positions for 8 Droplets at M_{RATIO} = 2.5

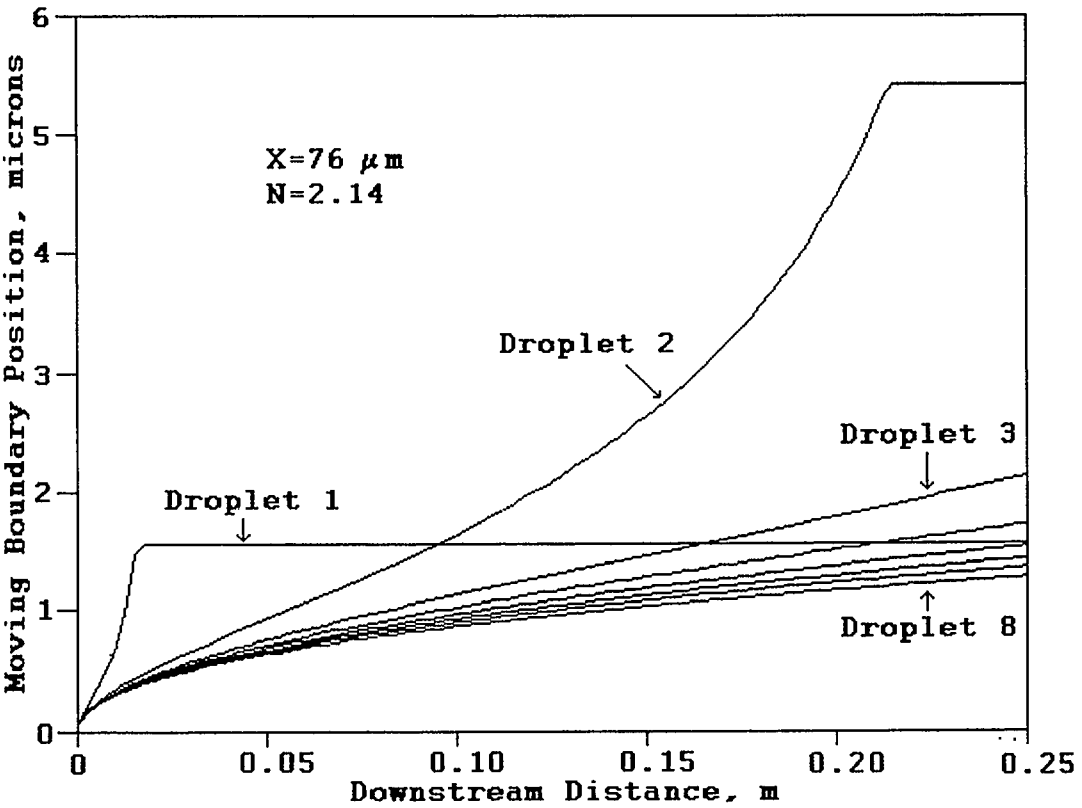

Figure 21: Reaction Front Positions for 8 Droplets at M_{RATIO} = 0.75

size. The curves which become flat are for droplets which have had 99.95% of their MEA consumed and so reaction front calculations are stopped. In both the figures this only occurs for the first droplet. As can be seen, for the larger droplets the reaction front positions are very close to one another, which indicates they behave like semi-infinite slabs.

In both figures the positions of the beginning of backwards motion of the reaction fronts of the largest droplets are indicated. In Figure 19 this phenomenon is clearly visible - the fronts for the two largest droplets can clearly be seen to have topped out and begun to come down. In Figure 20 it is not so clear, as the resolution of the graph is not high enough to show it. In both runs shortly after the start of regression of the reaction fronts, the calculations are stopped.

Figure 21 shows the reaction front positions of the same 8 droplets as Figure 20, with the difference being that M_{RATIO} is less than one. The chart illustrates what happens in this case. In the figure two of the eight droplets are completed. Due to the excess of H_2S in the system eventually all the droplets will be completely consumed. At distant times flat profiles of equal concentrations of H_2S will exist in all droplets.

6.4 Final Output

Graphs of the concentration of H_2S at the droplet

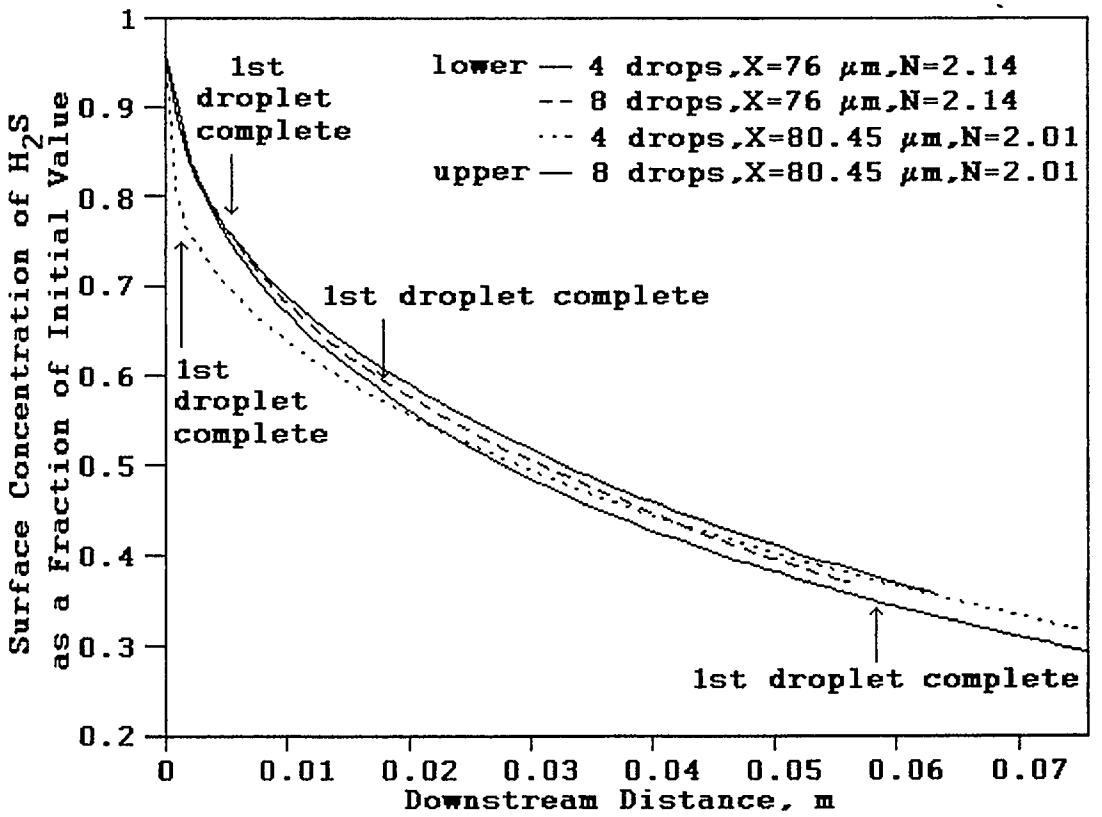

Figure 22: Results for Four Runs at M_{RATIO} = 2.5

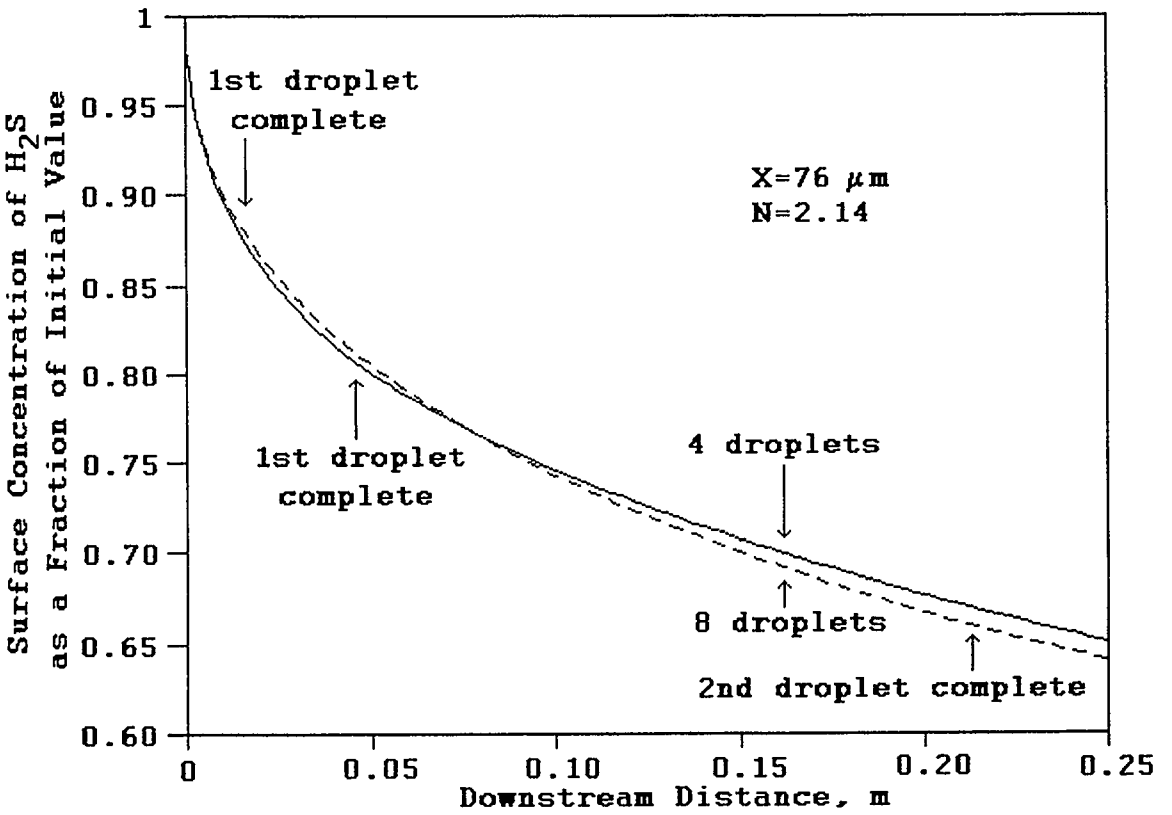

Figure 23: Results for Two Runs at M_{RATIO} = 0.75 .

surfaces as a fraction of the initial value against downstream distance travelled by the droplets are shown for the six runs in Figures 22 and 23. The ordinates of these curves are equal to the gas side concentration of H_2S as a fraction of the value in the feed, assuming that the solubility quantity K_{EQM} has not changed (which is reasonable for isothermal conditions and fairly low H_2S concentration in the feed). Also highlighted in the figures are where calculations are halted for droplets with more than 99.95% MEA consumption.

In Figure 22, the 4 runs can be grouped into two sets, each for a different spray, i.e. different combinations of the Rosin-Rammler parameters X and N. The first pair of runs in Figure 22 are for 4 and 8 droplets using X = 76 μm and N = 2.14. For the second pair of runs, values of X and N of 80.45 μm and 2.01 respectively are used.

Examining Figure 22, it is clear that all four runs produce quite similar results, and they are all quite remarkable - through only 5 to 6 cms of distance, more than 60% of the H_2S in the gas has been absorbed. The closeness of the curves to each other indicates that both the number of droplets calculated and the shape of the surface area distribution equation curve don't have a great effect on the final output, at least to the distance shown. The positions in the calculations where the first droplet for each run is completed are shown in the figure, and from the droplet profiles in Figures 10 - 13 it can be seen that they go in

order of diameter. The initial almost vertical drop in the curve for 4 drops, N = 2.01 can be attributed to the extremely fast mass transfer to the very small first droplet (1.25 μm). As soon as this droplet is consumed the curve shifts slope and heads back into the pack. At its end the curve seems to be crossing the corresponding curve for 8 drops.

The range of distances in the figure is quite short, only up to 7 cm. Of the four runs, three don't even make it this far. These premature stoppages are due to reaction front reversals in the largest droplets, which necessitated halting of the calculations. The curves initially run very steep, due to the extremely rapid mass transfer which results from the large driving forces. As these driving forces taper off, the slope of the curves decreases. If the curves were continued, they would eventually run asymptotic to a surface concentration of zero.

In Figure 23, the two runs are for 4 and 8 droplets, X = 76 μm and N = 2.14. The difference here is that the molar feed ratio M_{RATIO} is 0.75. As with the previous chart Figure 23 shows that the number of droplets computed does not significantly affect the results obtained. Also as in the case above, the 4 droplet curve here initially shows faster absorption due to the effect of the smallest droplet, an effect which goes away once the droplet is completed. As well, the curves are initially very steep, then taper off. If continued indefinitely, they would run asymptotic to a surface

concentration of something less than 0.25, at which point all the droplets would be complete. The reason the final value would be less than 0.25 is that an amount of the unconsumed H_2S would be physically absorbed into the droplets.

Comparing the curves with those in Figure 22, the significance of the value of M_{RATIO} to the calculations is obvious. In Figure 23 through 25 cms the surface concentration of H_2S has been reduced much less than it is in Figure 22 through less than 7 cm. For the same value of B^0 the larger value of M_{RATIO} means more liquid has been sprayed into the gas, so the reason for this is apparent. Hence it is clearly desirable to have the highest value of M_{RATIO} possible.

The difference in how the calculations for the two figures proceeded is apparent based on the distances the calculations were run through. For values of M_{RATIO} less than one, the limiting reagent in the system is MEA, so reaction front reversals do not take place and with the program as it is calculations can be continued indefinitely. With values greater than one however, the limiting reagant is the H_2S, and so depending on how much larger than one M_{RATIO} is sooner or later the reaction fronts in the droplets are going to reverse and the calculations will have to be stopped.

6.5 Inputs

The system characterizing inputs that are used in the sample runs of the program are chosen to represent typical

values that would exist in an actual Waterloo scrubber. These inputs include the component diffusivities, the Rosin-Rammler parameters, and the concentration and feed ratios. For the specific application the program is written for, the range of possible values for these inputs are fairly limited. Clearly the diffusivities of the two components are not going to change, and for the Rosin-Rammler parameters the specific values will vary, but the range of Sauter mean diameters they represent will be close to that used here. It would of course be desirable to use smaller droplets as they would result in faster mass transfer, but the additional energy requirements make this option unattractive.

The two inputs which can vary are the maximum concentration ratio (B^0/A^*) and the molar feed ratio M_{RATIO}. In practise it is desirable to make M_{RATIO} as large as possible, but the problem is that if the H_2S content of the feed gas is quite high, very large volumes of scrubbing solution would have to be sprayed. Turbotak indicates that L/G ratios in their units vary from about 1 to around 5 U.S. gal/1000 ft^3 gas, with a recommended value around 2 (Spink, D.R., 1992). The L/G ratios (in the same units) in this system are given by:

$$L/G = 7.48 \frac{M_{RATIO}}{B^0/A^*} \qquad (52)$$

Thus for the runs in Figure 22, L/G = 2.49, and for the runs in Figure 23 L/G = 0.748. Both of these values are then

reasonable. To maintain a high M_{RATIO} and reduce the amount of liquid to be sprayed, it might be desirable to increase the feed concentration of MEA, B^0. This would create other problems of course, including increased difficulties with corrosion. This possibility, combined with the certainty that feed H_2S concentrations would be different that the value assumed here, make B^0/A^* the least predictable input. The effect of increasing this value would be roughly the same as reducing the diffusivity ratio, to reduce the rate of reaction and hence the rate of absorption of H_2S. Decreasing the value would of course have the opposite effect.

Inputs which are noteable by their absence are the inside pipe diameter D_{PIPE} and the solubility quantity K_{EQM}. The first is not needed due to the calculations being intensive, but of course if the total amount of H_2S absorbed was desired it would have to be known. The second quantity is left to the user to find for himself; it is needed to calculate a value for A^* from the partial pressure of H_2S in the feed. Leaving it out of the program simplifies things considerably.

If it is desired to use an amine other than MEA in the scrubbing liquid, for the most part the only changes that would have to be made are in the inputs. The value of the amine diffusivity D_2 would be different, and accordingly so would the value of D_1/D_2. The concentration of the amine in the feed B^0 would also be different, affecting the value of B^0/A^*. A different molar feed ratio M_{RATIO} is also possible. If

the reaction stoichiometry of the amine with H_2S is not 1 - 1, then the program itself would have to be slightly modified.

6.6 Calculation Times

A table of run times for the 6 runs of Figures 22 and 23 are presented in Table 2. In examining the times it is clear there are aberrations determined by how busy the system was when the runs were performed, as well as how far the calculations went before stopping. However, overall the table shows that in general it takes less time to calculate fewer droplets, all other things being held the same. The major

Table 2: Calculation Times

Run	Time (hr)	$(N_{IVAL})_1$	$\sum_{K=1}^{N_{DROP}} (N_{IVAL})_K$
4 drops, N = 2.14 in Fig. 22	2.62	225	5949
8 drops, N = 2.14 in Fig. 22	3.68	125	10945
4 drops, N = 2.01 in Fig. 22	62.08	100	15198
8 drops, N = 2.01 in Fig. 22	4.32	75	11585
4 drops in Fig. 23	1.72	150	3964
8 drops in Fig. 23	10.08	75	6563

exception to this is for the run of 4 droplets for the Rosin-Rammler parameters of X = 80.45 μm and N = 2.01. The reason for this can be seen by examining the fourth column in the table, which shows the sum of the number of space intervals for all the droplets. Every time step this is the total number of concentration values which must be computed, and is also

the number of intervals that must be numerically integrated through. This number combines the effects of the number of droplets, the number of space intervals for the smallest droplet, and the specifics of the droplet size distribution. The largest value is for the third run in the table, which is the run which took the longest time. It is even larger than the value for the same Rosin-Rammler parameters, with twice as many droplets. The reason it is so large is a result of the peculiar shape of the surface area distribution equation for that set of Rosin-Rammler parameters - the peak is very close to zero. The consequence of this is that the smallest droplet is very small relative to the other droplets, resulting in the number of intervals for the larger droplets being extremely large.

The third column in Table 2 shows for each run the number of intervals the radius of the smallest droplet is subdivided into, which is part of the input. This value is significant in that by equations 25 and 29 it determines the size of the time step, as $(\Delta z)_1$ is the reciprocal of $(N_{IVAL})_1$. Hence the larger this value is the smaller the time step size is. Calculation times can be reduced by reducing this value, but the tradeoff is accuracy. One possible answer to this problem is the use of implicit methods in the discretization of the differential equations. Such methods are stable for any time step size. In the use of such methods time steps would still have to be kept small however, to keep accurate track of reaction front

positions and the outside H_2S concentration.

Another issue arising from the discussion of calculation times is the effect adding further complexity to the system model would have. More complexity means more calculations, which means more time, and with some runs already taking more than two days, this is a somewhat daunting prospect. Not only would calculations take longer but debugging the resulting more complex program would be accordingly more difficult, as the possibility that the calculations would take unforseen turns after running for a long time could be higher.

6.7 Errors and Accuracy

No discussion of the results of a numerical calculation is complete without reference to the errors in the calculation. The discretization of the differential equations uses derivative approximations which are in error of the order of $(\Delta\tau)_k$ and $[(\Delta z)_k]^2$, and the numerical integration routine for the H_2S mass balance is in error of the order of $[(\Delta z)_k]^4$. And of course there are additional errors associated with the use of the Lagrange polynomials and in the convergence of the reaction front positions. These errors can be reduced by reducing the grid widths in both space and time, but as previously mentioned the price is increased calculation times. As a test of the accuracy of the results in Figures 22 and 23, the run from Figure 22 for 4 droplets at X = 76 and N = 2.14 was performed with more than 50% more space intervals for the

smallest droplet (350) and a 30% smaller time step. The results from the two runs are shown in Figure 24 for comparison. In Figure 24 the line is for the original run, and the points are for the new run. As can be seen the two exactly overlap, which indicates that the results in Figures 22 and 23 are accurate.

As a further test of the accuracy of the results of the computer program, the program was modified to calculate the problem of absorption plus instantaneous reaction in a semi-infinite slab (Danckwerts' problem) and the results compared to the known analytical solution to this problem (shown in Appendix A). The comparison is shown in Figure 25. In the chart the curves represent the result of the numerical calculations, and the points the analytical solution to the problem for the same absolute time. Runs were performed for times of 1 s and 5 s after the start of mass transfer, using as inputs the same values used previously in the set of 6 runs. As can be seen for both times the numerical results very closely correspond to the analytical results. This indicates the accuracy of the differential equation solving procedure in the program.

There are only two known inaccuracies in the program. The first is with the mass balance step, in which for each droplet the updated concentration profiles are numerically integrated, but the H_2S concentration at the surface is the old value calculated from the previous time step. So the new computed

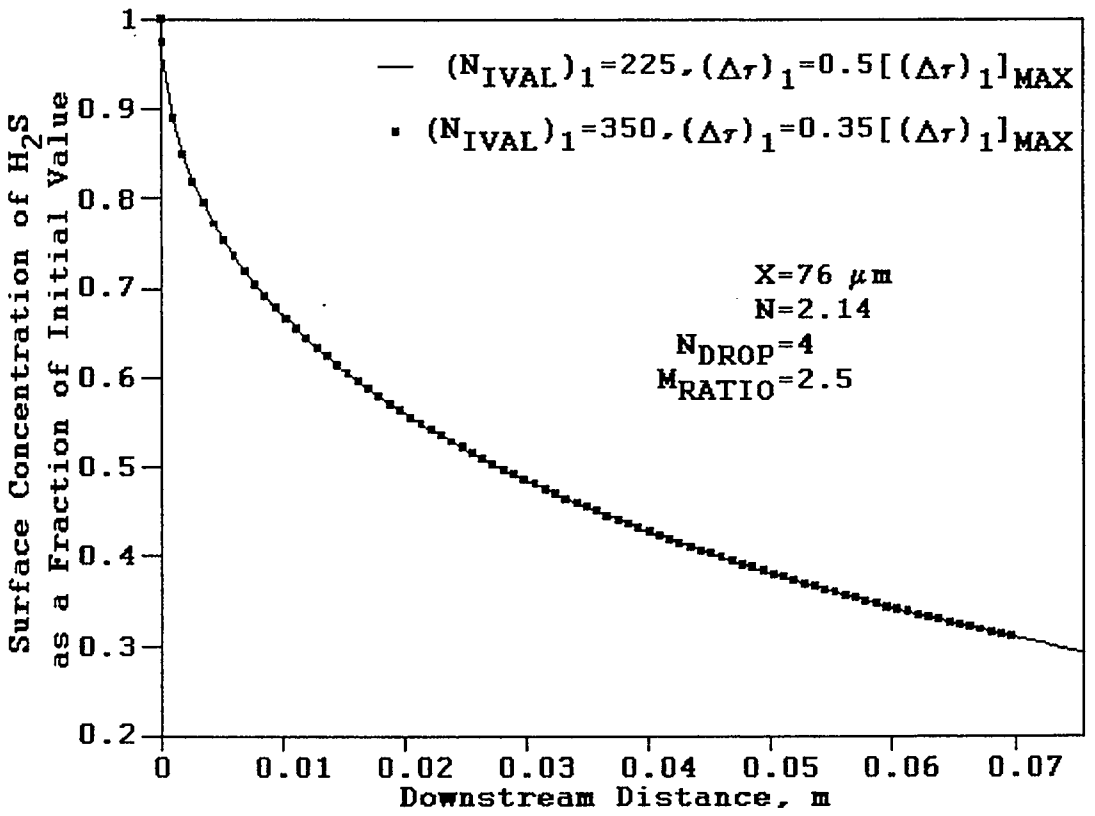

Figure 24: Accuracy Test for Results

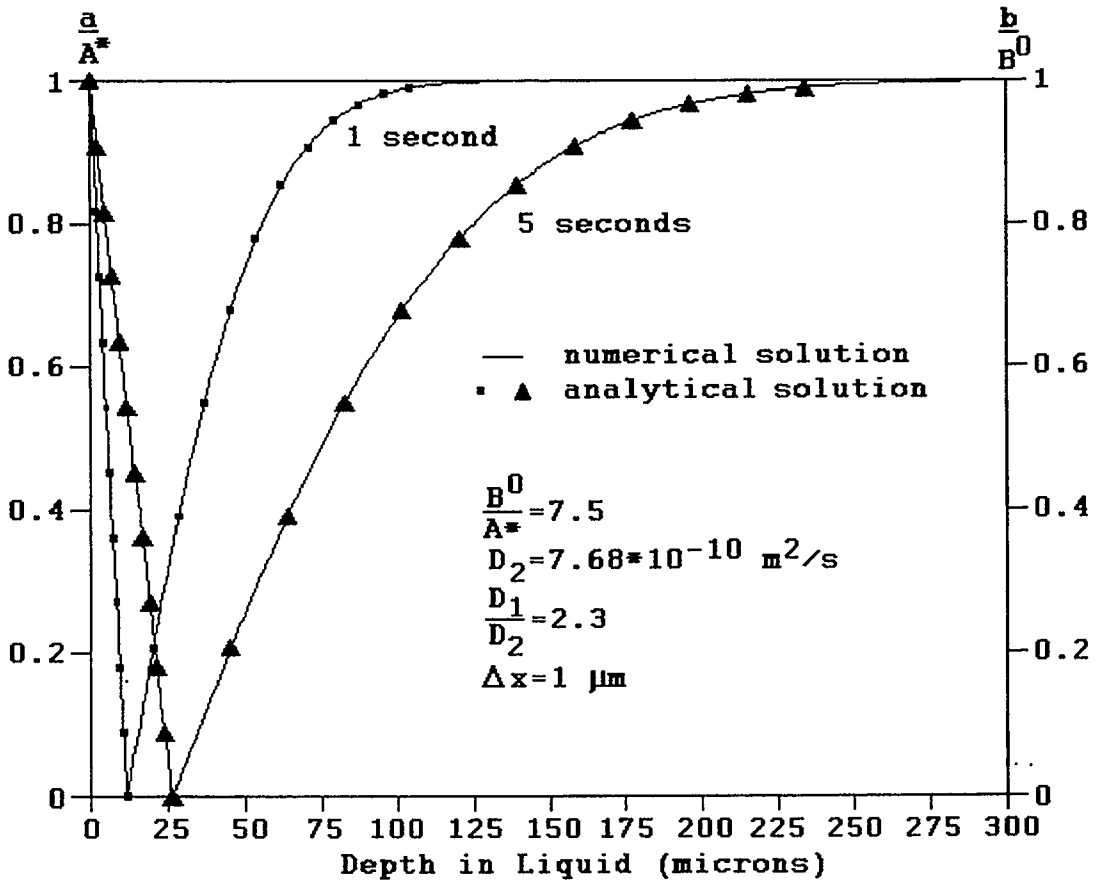

Figure 25: Numerical Solution of Danckwerts' Problem

value of the H_2S surface concentration is slightly off, but to find the true value an iterative procedure would have to be used, which is considered unnecessary. The other problem is with droplets for which more than 99.95% of the MEA has been consumed. For these droplets calculations of the MEA profiles are stopped, which of course neglects what happens afterwards. Both of these problems have very little impact on results.

No experimental results exist with which to compare the results, as these would be quite difficult to attain and would have to be for a chemical absorption system involving instantaneous reaction. However, if there were, the results obtained from the program as shown in Figures 22 and 23 would be too high in comparison. This can be attributed not to inaccuracies in the calculations but in the model. The assumption of a flat H_2S concentration profile in the gas phase is what would cause the results to be furthest off. In a real system the H_2S concentration at the surface of the droplets would certainly be less than in the bulk of the gas, and hence the driving force for absorption would be less. This would result in longer times for absorption. To increase the reliability of the model, this assumption should be replaced with a convective mass transfer model such as the film theory. Increasing the number of droplet sizes computed would also improve the reliability of results, but as can be seen from Figures 22 and 23, it wouldn't necessarily change the output significantly.

CHAPTER 7

CONCLUSIONS AND RECOMMENDATIONS FOR FUTURE WORK

In this thesis a model of chemical absorption of H_2S by an amine - containing spray was presented. The governing diffusion equations in spherical coordinates were given, setting up a moving boundary problem. Details of how the spray was discretized into a finite number of droplet sizes were presented, and the H_2S mass balance procedure outlined. How the model was to be solved was covered next, including the development of the finite difference approximations to the differential equations. The idea of drawing an analogy between the sphere at short times and a semi-infinite slab allowed the calculation of initial profiles in the droplets, and then the specific mass balance equation was given. The computer program written to solve the model was then presented, with the major point of interest being the marching method used to increment reaction front positions across space grid lines.

Results from a number of runs on the program were examined. The trends of the calculations were shown to be dependent on the value of M_{RATIO} used in the calculations. For values greater than 1, mass transfer was extremely fast, with more than 60% of the H_2S originally present being absorbed in less than 10 cm in the cases examined. However, due to regression of the reaction fronts of the largest droplets, the calculations could not be carried out for long times. For

values less than 1, calculations could be continued indefinitely, and they showed rapid mass transfer but not as rapid as before. It was also learned that using more droplets in the calculations does not give significantly different results, and does not necessarily require more time to compute. The results obtained were shown to be accurate, but they are not believed to be entirely reliable. Due to the trivialization of the gas phase mass transfer, the results are believed to be overly generous.

Overall a fairly successful computer program has been written which can estimate the chemical absorption of H_2S by an amine - containing spray, if the value of the molar feed ratio of the amine to the H_2S is less than 1 and the amine has a 1 - 1 stoichiometry with H_2S. The program can also be extended to gas streams containing CO_2 if the amine used is one which selectively absorbs H_2S over CO_2, for example TEA or MDEA. Application to the absorption of SO_2 by an amine spray is also possible (Spink, D.R., 1992). The trends shown are positive enough to warrant further work. Recommendations for future work are as follows:

1. A reverse marching method procedure should be added to the computer program so that the regression of reaction fronts can be calculated for cases when M_{RATIO} is greater than one.
2. A convective mass transfer model for the gas phase should be added to make the results more realistic.

3. If possible, the initial region of the scrubber with the expanding gas jet should be modelled. The outside H_2S concentration and droplet concentration profiles obtained from this could then be used as initial conditions for the current program, giving a complete model of the Waterloo scrubber.

BIBLIOGRAPHY

Brena de la Rosa, A., Measurement of the Drop Size Distributions for 3 Caldyn Nozzles, internal report, Thermal Engineering Group, Department of Mechanical Engineering, University of Waterloo, Waterloo ON, 1987.

Chuang, Y.K., and J. Szekely, "On the Use of Green's Functions for Solving Melting or Solidification Problems", Int. J. Heat Mass Transfer, vol. 14, pp. 1285-1294, 1971.

Clift, R., J.R. Grace, and M.E. Weber, Bubbles, Drops and Particles, Academic Press, New York, 1978.

Crank, J., Free and Moving Boundary Problems, Oxford Science Publications, Toronto, 1984.

Danckwerts, P.V., Gas-Liquid Reactions, McGraw-Hill, New York, 1970.

Danckwerts, P.V., and M.M. Sharma, "The Absorption of Carbon Dioxide into Solutions of Alkalis and Amines", The Chemical Engineer, no. 202, pp. 244-280, Oct. 1966.

Dewynne, J.N., and J.M. Hill, "Integral Formulations and Bounds for Two Phase Stefan Problems Initially not at Their Fusion Temperature", Acta Mechanica, vol. 58, pp. 201-228, 1986.

Dullien, F.A.L., and D.R. Spink, U.S. Patent 4,067,703, 1978.

Dursunkaya, Z., and S. Nair, "A Moving Boundary Problem in a Finite Domain", Trans. ASME, vol. 57, pp. 50-56, March 1990.

Elghobashi, S.E., G.S. Samuelsen, J.E. Wuerer, and J.C. LaRue, "Prediction and Measurement of Mass, Heat, and Momentum Transport in a Nonreacting Turbulent Flow of a Jet in an Opposing Stream", J. Fluids Eng., vol. 103, pp. 127-132, March 1981.

Gluckert, F.A., "A Theoretical Correlation of Spray-Dryer Performance", A.I.Ch.E. J., vol. 8, no. 4., pp. 460-466, Sept. 1962.

Gnyp, A.W., C.C. St. Pierre, D.S. Smith, and S. Raman, Experimental Optimization of the Liquid Injection System in a Venturi Scrubber, report prepared for the Ontario environment ministry, Department of Chemical Engineering, University of Windsor, Windsor ON, 1980.

Hill, J.M., and J.N. Dewynne, "Improved Lower Bounds for the Motion of Moving Boundaries", J. Austral. Math. Soc. Ser. B, vol 26, pp. 165-175, 1984.

ibid., "Some Recent Results for Heat-Diffusion Moving Boundary Problems", Bull. Austral. Math. Soc., vol. 32, pp. 437-460, 1985.

Jenson, V.G., and G.V. Jeffreys, Mathematical Methods in Chemical Engineering, Academic Press, New York, 1963, pp. 151-154.

Kohl, A.L., and F.C. Riesenfeld, Gas Purification, 3rd. ed., Gulf Publishing, 1979.

Kulic, E., An Experimental and Theoretical Study of Simultaneous Heat and Mass Transfer Applied to Steam Dousing, Ph.D. Dissertation, Department of Chemical Engineering, University of Waterloo, Waterloo ON, 1976.

Levich, V.G., Physicochemical Hydrodynamics, Prentice-Hall, 1962, pp. 34-37, 586-600.

Lukashev, V.K., "Jet Model of Spray Cone in a Pneumatic Nozzle", translated from Teoreticheskie Osnovy Khimicheskoi Tekhnologii, vol. 22, no. 2, pp. 218-225, March-April 1988.

Masters, K., Spray Drying, Leonard Hill Books, London, 1972.

Masters, K., "Spray Drying, The Unit Operation Today", Ind. Eng. Chem., vol. 60, no. 10, pp. 53-63, Oct. 1968.

Mugele, R.A., and H.D. Evans, "Droplet Size Distributions in Sprays", Ind. Eng. Chem., vol. 43, no. 6, pp. 1317-1332, 1951.

Ockendon, J.R., and W.R. Hodgkins, eds., Moving Boundary Problems in Heat Flow and Diffusion, Clarendon Press, Oxford, 1974.

Patience, G.S., Numerical Solutions for Laminar Forced Convection and Fluid Flow in Pipes, M.Sc. Thesis, Department of Chemical Engineering, Faculty of Engineering, The University of Calgary, 1987.

Pedroso, R.I., and G.A. Domoto, "Inward Spherical Solidification - Solution by the Method of Strained Coordinates", Int. J. Heat Mass Transfer, vol. 16, pp. 1037-1043, 1973.

Perry, R.H., D.W. Green, and J.O. Maloney, eds., Perry's

Chemical Engineers' Handbook, 6th ed., McGraw-Hill, New York, 1984, pp. 5-22, 8-5, 20-90.

Press, W.H. B.P. Flannery, S.A. Teukolsky, and W.T. Vetterling, Numerical Recipes, Cambridge University Press, New York, 1986, pp. 156-163.

Ranz, W.E., and W.R. Marshall, Jr., "Evaporation From Drops", Chem. Eng. Progr., vol 48., no. 3, pp. 141-146, 173-180, March 1952.

Rhodes, E., Turbulent Mass Transport From an Interface, Ph.D. Dissertation, Department of Chemical Engineering, Faculty of Technology, Victoria University of Manchester, 1964.

Riley, D.S., F.T. Smith, and G. Poots, "The Inward Solidification of Spheres and Circular Cylinders", Int. J. Heat Mass Transfer, vol. 17, pp. 1507-1516, 1974.

Smith, G.D., Numerical Solution of Partial Differential Equations, Oxford University Press, Toronto, 1965.

Soward, A.M., "A Unified Approach to Stefan's Problem for Spheres and Cylinders", Proc. R. Soc. Lond. A, vol. 373, pp. 131-147, 1980.

Spink, D.R., "Handling Mists and Dusts", Chemtech, vol. 18, no. 6, pp. 364-368, June 1988.

ibid., private communication with E. Rhodes, June 23, 1992.

Spink, E.F., D.R. Spink, J.E. Browne, and P. Lamarche, "Control of Carbon Particle Emissions From a Pulp Mill Refuse-Fueled Boiler by Wet Scrubbing", Pulp & Paper Canada, vol. 88, no. 5, pp. 47-49, 1987.

Spink, E.F., and R.F. Spink, "Pulp Mill Applications of Waterloo Scrubber Technology", Pulp & Paper Canada, vol. 89, no. 12, pp. 147-150, 1988.

Swaddle, T.W., Applied Inorganic Chemistry, lecture notes for CHEM 429, Department of Chemistry, Faculty of Science, University of Calgary, 1986.

Treybal, R.E., Mass-Transfer Operations, 3rd ed., McGraw-Hill, 1987.

Turbotak Nozzles, pamphlet, Turbotak Inc., Waterloo ON Canada.

Voller, V., and M. Cross, "Accurate Solutions of Moving Boundary Problems Using the Enthalpy Method", Int. J. Heat Mass Transfer, vol 24, pp. 545-556, 1981.

Wankat, P.C., Equilibrium Staged Separations, Elsevier, New York, 1988.

Weast, R.C., and M.J. Astle, eds., CRC Handbook of Chemistry and Physics, 63rd ed., CRC Press, Boca Raton, 1982.

Yakowitz, S., and F. Szidarovszky, An Introduction to Numerical Computations, 2nd ed., Macmillan, New York, 1989.

Younger, A.H., Natural Gas Processing Principles and Technology, lecture notes for ENCH 607 and ENCH 609, Department of Chemical Engineering, Faculty of Engineering, University of Calgary, 1977.

APPENDIX A

DANCKWERTS' PROBLEM

The problem (Danckwerts, pg. 38, 1970):

$$D_1\frac{\partial^2 a}{\partial x^2}=\frac{\partial a}{\partial t} \quad 0<x<\lambda;\ \begin{matrix} x=0, a=A^*, t>0 \\ x=\lambda, a=0, t>0 \end{matrix} \tag{A1}$$

$$D_2\frac{\partial^2 b}{\partial x^2}=\frac{\partial b}{\partial t} \quad x>\lambda;\ \begin{matrix} t=0, b=B^0, x>0 \\ x=\lambda, b=0, t>0 \\ x=\infty, b=B^0, t>0 \end{matrix} \tag{A2}$$

$$-D_1\frac{\partial a}{\partial x}\Big|_\lambda = D_2\frac{\partial b}{\partial x}\Big|_\lambda \quad t>0;\ t=0, \lambda=R \tag{A3}$$

Equations A1 and A2 are solved by the method of combination of variables, combining one time condition and one boundary condition together. As a result of solving for the unknown constants of integration, λ is found to be directly proportional to the square root of time. For simplicity, the following form is assumed:

$$\lambda=2\sqrt{\alpha t} \tag{A4}$$

Thus the solution is:

$$a(x,t)=A^*\left[1-\frac{erf\left(\frac{x}{2\sqrt{D_1 t}}\right)}{erf\sqrt{\frac{\alpha}{D_1}}}\right] \quad 0\le x\le 2\sqrt{\alpha t} \tag{A5}$$

$$b(x,t)=B^0\left[1-\frac{erfc\left(\frac{x}{2\sqrt{D_2 T}}\right)}{erfc\sqrt{\frac{\alpha}{D_2}}}\right] \quad x\ge 2\sqrt{\alpha t} \tag{A6}$$

The value α is a parameter found by substituting the above

results into equation A3, which yields:

$$e^{\alpha\left(\frac{1}{D_2}-\frac{1}{D_1}\right)}\frac{erfc\sqrt{\frac{\alpha}{D_2}}}{erf\sqrt{\frac{\alpha}{D_1}}}=\frac{B^0/A^*}{\sqrt{D_1/D_2}} \qquad \text{(A7)}$$